NeuroImage 264 (2022) 119671

Contents lists available at ScienceDirect

NeuroImage

journal homepage: www.elsevier.com/locate/neuroimage

Correspondence between gene expression and neurotransmitter receptor and transporter density in the human brain

Justine Y. Hansen[a,*], Ross D. Markello[a], Lauri Tuominen[b], Martin Nørgaard[c,d], Elena Kuzmin[e,f], Nicola Palomero-Gallagher[g,h,i], Alain Dagher[a], Bratislav Misic[a]

[a] McConnell Brain Imaging Centre, Montréal Neurological Institute, McGill University, Montréal, Canada
[b] Department of Psychiatry, The Royal's Institute of Mental Health Research, University of Ottawa, ON, Canada
[c] Neurobiology Research Unit & CIMBI, Copenhagen University Hospital, Copenhagen, Denmark
[d] Center for Reproducible Neuroscience, Department of Psychology, Stanford University, Stanford, California, USA
[e] Department of Biology, Centre for Applied Synthetic Biology, Concordia University, Montréal, Canada
[f] Department of Human Genetics, Rosalind & Morris Goodman Cancer Institute, McGill University, Montréal, Canada
[g] Institute of Neuroscience and Medicine (INM-1), Research Centre Jülich, Germany
[h] Department of Psychiatry, Psychotherapy and Psychosomatics, Medical Faculty, RWTH, Aachen, Germany
[i] C. and O. Vogt Institute for Brain Research, Heinrich-Heine-University Düsseldorf, Düsseldorf, Germany

A B S T R A C T

Neurotransmitter receptors modulate signaling between neurons. Thus, neurotransmitter receptors and transporters play a key role in shaping brain function. Due to the lack of comprehensive neurotransmitter receptor/transporter density datasets, microarray gene expression measuring mRNA transcripts is often used as a proxy for receptor densities. In the present report, we comprehensively test the spatial correlation between gene expression and protein density for a total of 27 neurotransmitter receptors, receptor binding-sites, and transporters across 9 different neurotransmitter systems, using both PET and autoradiography radioligand-based imaging modalities. We find poor spatial correspondences between gene expression and density for all neurotransmitter receptors and transporters except four single-protein metabotropic receptors (5-HT_{1A}, CB_1, D_2, and MOR). These expression-density associations are related to gene differential stability and can vary between cortical and subcortical structures. Altogether, we recommend using direct measures of receptor and transporter density when relating neurotransmitter systems to brain structure and function.

1. Introduction

Neurotransmitter receptors and transporters support synaptic communication, regulating signal transmission from neuron to neuron. As such, regional variation of receptor and transporter distributions shapes the functional specialization of the brain (Froudist-Walsh et al., 2021; Goulas et al., 2021; Palomero-Gallagher and Zilles, 2019; Shine, 2019; Suárez et al., 2020; Zilles and Palomero-Gallagher, 2017). Recent studies have investigated how receptor information can tune computation models, and how receptors, as well as excitatory-inhibitory ratio, are related to neurodevelopment, cognition, neural dynamics, and disease (Deco et al., 2020; Hoftman et al., 2018; Larsen et al., 2021; Preller et al., 2018; Shine et al., 2019). However, due to the lack of comprehensive neurotransmitter receptor and transporter density datasets (open-source or otherwise), receptor/transporter densities are often substituted with microarray gene expression from the Allen Human Brain Atlas (AHBA) (Hawrylycz et al., 2012), under the assumption that levels of gene expression are correlated with cell surface protein abundance (Ballentine et al., 2021; Braun et al., 2021; Burt et al., 2018; 2021; Chang et al., 2022; Deco et al., 2020; Fulcher et al., 2019; Gao et al., 2020; Hoftman et al., 2018; Larsen et al., 2021; Preller et al., 2018; 2020; Shine et al., 2019).

Despite the frequent use of receptor/transporter densities with gene expression, the assumed topographical correlation between gene expression and receptor/transporter density has yet to be comprehensively and formally tested across multiple neurotransmitter systems and imaging modalities. Indeed, there are several reasons gene expression may not be correlated with receptor density. First, microarray gene expression measures the outcome of gene transcription and the abundance of mRNA, not levels of protein. Importantly, levels of mRNA and protein are often not correlated, even within the same tissue (Mühleisen et al., 2021; Schwanhäusser et al., 2011). Second, several steps are involved between protein translation and expression of the receptor/transporter on the cell surface, including post-translational modifications, protein folding, and reaching a designated cellular target. Variations in the activity of these processes will affect receptor/transporter density. Additionally, in

* Corresponding author.
E-mail addresses: justine.hansen@mail.mcgill.ca (J.Y. Hansen), bratislav.misic@mcgill.ca (B. Misic).

https://doi.org/10.1016/j.neuroimage.2022.119671.
Received 11 July 2022; Received in revised form 29 September 2022; Accepted 5 October 2022
Available online 6 October 2022.

the case of receptors and transporters that are expressed far from the cell nucleus, there is a spatial mismatch between levels of gene expression and protein abundance. Third, multiple genes in the Allen Human Brain Atlas show high inter-subject variability, indicating the possible unreliability of such group-averaged expression levels. Fourth, the concordance between gene expression and protein density may not be spatially homogeneous in the brain. Altogether, a comprehensive study mapping receptor/transporter densities and gene expression levels is necessary to determine whether neurotransmitter receptors and transporters show expression-density associations in the human cortex.

Whether AHBA-derived gene expression can predict neurotransmitter receptor densities across the cortex was first formally tested by Rizzo et al. (2014). Rizzo et al. found a close relationship between *HTR1A* gene expression and 5-HT_{1A} PET tracer affinity, but no relationship between opioid receptor gene expression (mu, kappa, and delta) and [^{11}C]diprenorphine, a PET tracer that binds to all three opioid receptor subtypes. This served as an initial indication that the topographic relationship between microarray gene expression and receptor density is more complex than appreciated by the neuroimaging field. Future studies then tested specific receptor systems (i.e. serotonin (Beliveau et al., 2017; Komorowski et al., 2017) and $GABA_A$ (Nørgaard et al., 2021)), and found that gene expression was not always a good predictor of receptor density. With recently available multisystem receptor density datasets from both autoradiography (Zilles and Palomero-Gallagher, 2017) and PET (Dukart et al., 2021; Hansen et al., 2021), as well as a better understanding of how to best process gene expression data from the Allen Human Brain Atlas (Arnatkevičiūtė et al., 2019; Markello et al., 2021), a comprehensive account for how gene expression and receptor density relate to one another across multiple neurotransmitter systems and imaging modalities is possible (Murgaš et al., 2022).

Here we investigate whether microarray gene expression can be used to estimate neurotransmitter receptor/transporter densities in the cortex. To measure gene expression levels, we use the Allen Human Brain Atlas that code for specific neurotransmitter receptors or transporters (Hawrylycz et al., 2012; Markello et al., 2021). Additionally, we use both positron emission tomography (PET)- and autoradiography-derived measures of neurotransmitter receptor densities for a total of 27 neurotransmitter receptors and transporters across 9 different neurotransmitter systems (Aghourian et al., 2017; Bedard et al., 2019; Beliveau et al., 2017; Ding et al., 2010; DuBois et al., 2016; Dukart et al., 2018; Gallezot et al., 2010; Hillmer et al., 2016; Kaller et al., 2017; Kantonen et al., 2020; Naganawa et al., 2021; Nørgaard et al., 2021; Normandin et al., 2015; Parker et al., 2015; Sandiego et al., 2015; Savli et al., 2012; Smart et al., 2019; Zilles and Palomero-Gallagher, 2017). To ensure results are not biased by methodological choices, we repeat our analyses using RNAseq data, in a separate parcellation resolution, and use a conservative spatial autocorrelation-preserving null model (Alexander-Bloch et al., 2018; Markello and Misic, 2021). We find that measures of gene expression can generally not be used as a proxy for receptor nor transporter density except for a select few neurotransmitter receptors: 5-HT_{1A} (serotonin), D_2 (dopamine), and MOR (opioid). Finally, we provide evidence that the link between receptor/transporter density and gene expression is related to inter-subject genetic variability.

2. Results

The present report uses the following three datasets to assess the gene expression-protein density relationship for 27 receptors and transporters: (1) the Allen Human Brain Atlas, which remains the most spatially comprehensive dataset measuring human brain gene expression (Hawrylycz et al., 2012), (2) a PET atlas which, to our knowledge, is the most extensive collection of open-access receptor and transporter densities in the brain (Hansen et al., 2021), and (3) the autoradiography dataset from Zilles and Palomero-Gallagher (2017) which is the only multi-receptor-system autoradiography dataset and the most spatially specific mapping of receptors in the human brain.

Gene expression-protein density correspondence

Using the group-averaged healthy control PET-derived neurotransmitter receptor and transporter densities, we find that in many cases, there is no close correspondence between receptor density and receptor gene expression (Fig. 1; for results using RNAseq data, see Fig. S1). Indeed, only seven proteins (5-HT_{1A}, 5-HT_{2A}, CB_1, D_2, H_3, M_1, MOR) show significant (one-tailed $p_{spin} < 0.05$) and large ($r > 0.5$) relationships with the expression of their corresponding genes (*HTR1A, HTR2A, CNR1, DRD2, HRH3, CHRM1, OPRM1*, respectively). Similarly, using the autoradiography dataset, we find that in almost all cases, gene expression is a poor approximator of neurotransmitter receptor density (Fig. 2; for results across three laminar layers, see Fig. S2, and for results using RNAseq data, see Fig. S3). We again find a close correspondence between 5-HT_{1A} and the expression of *HTR1A* ($r = 0.80$, $p_{spin} = 0.0003$). However, unlike what was observed with the PET dataset, M_1 does not show any correlations with *CHRM1*. Finally, we note that some gene-receptor pairs show significant but low ($r < 0.5$) expression-density correlations, namely: *HTR4*–5-HT_4 (PET), *CHRM3*–M_3 (autoradiography), and *ADRA2A*–α_2 (autoradiography).

To ensure results are not influenced by the choice of brain parcellation, we repeated the PET analyses in a finer parcellation of 111 left hemisphere cortical regions (Fig. S4; (Cammoun et al., 2012)). At this higher resolution, we find that only 5-HT_{1A}, CB_1, D_2, and MOR still show close correspondence with their associated genes. H_3 is no longer significantly correlated with *HRH3* ($r = 0.47$, $p_{spin} = 0.13$), M_1 and 5-HT_{2A} are significantly correlated with their associated genes, although to a lesser degree ($r = 0.38$, $p_{spin} = 0.005$ and $r = 0.38$, $p_{spin} = 0.013$, respectively). 5-HT_4 is now better correlated with *HTR4* than before ($r = 0.54$, $p_{spin} = 0.003$), and $mGluR_5$ is now significantly correlated with *GRM5*, although not strongly ($r = 0.39$, $p_{spin} = 0.008$). The presence of an additional significant correlation ($mGluR_5$) and an improved correlation (5-HT_4) suggests that a finer parcellation (alongside more precise measurements) may provide a more optimistic account of the relationship between gene expression and receptor density. Altogether, 5-HT_{1A}, CB_1, D_2, and MOR show stable and high expression-density correspondence across both spatial scales and imaging modalities. The edge-cases (i.e. 5-HT_{1B}, 5-HT_{2A}, 5-HT_4, H_3, M_1, M_3, $mGluR_5$, α_2) may represent receptors where there is a biologically close relationship between gene transcription and protein abundance, but due to measurement error or individual variability, receptor density cannot be adequately predicted by AHBA gene expression.

Next, we consider whether gene expression and receptor densities show similar association patterns in the subcortex (Fig. 3). We focus on fifteen subcortical structures, including the brainstem and seven pairs of homologous brain regions. Note that we separate subcortical and cortical analyses in the main text, but the combined model is shown in Fig. S8. Tracers used in the subcortex are the same as those used in the cortex except for D_2, where [^{11}C]raclopride is used in the subcortex in favour of [^{11}C]FLB-457 (Dagher and Palomero-Gallagher, 2020). Unlike in the cortex, we find a high correlation between D_1 subcortical gene expression and receptor density ($r = 0.87$, $p < .001$), which may be reflective of nonspecific D_1 binding in the cortex (Ekelund et al., 2007). We also find a high expression-density correlation for VAChT, which may reflect the greater transporter availability in the subcortex. Meanwhile, receptors with high expression-density associations in the cortex generally show similarly high relationships in the subcortex, with the exception of MOR for which the expression-density relationship decreases ($r = 0.85$ in the cortex, $r = 0.53$ in the subcortex) despite greater receptor availability. Altogether, we find preliminary evidence that the relationship between gene expression and receptor density may vary between the cortex and subcortex, although this analysis should be replicated in future work using a finer parcellation and more sensitive measurements.

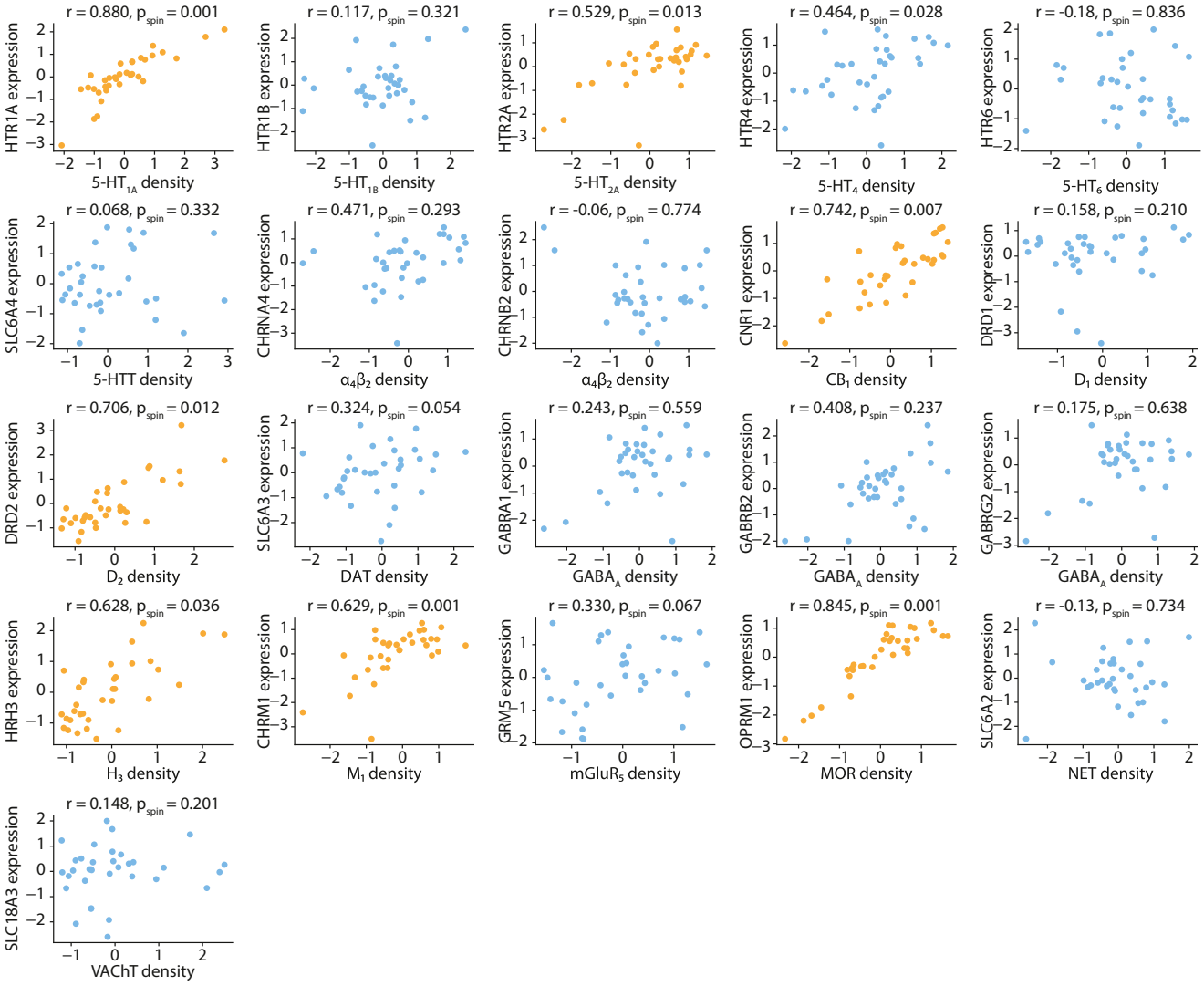

Fig. 1. PET-derived receptor/transporter densities versus gene expression | PET tracer maps for 18 different neurotransmitter receptors and transports reveal that the density of only five neurotransmitter receptors correlates significantly with the expression of their corresponding gene (Spearman r), across 34 Desikan Killiany regions in the left cortex. Yellow scatter plots indicate significant ($p_{spin} < 0.05$) and large ($r > 0.5$) expression-density correspondence. Receptor density and gene expression is z-scored.

Potential mechanisms underlying low associations

We next sought to understand why certain neurotransmitter receptors demonstrate expression-density correspondence, whereas other receptors, and all transporters, show no expression-density correspondence. Since group-averaged measures of gene expression and receptor/transporter density come from disjoint samples of participants, we hypothesized that inter-subject variability might distort the relationship between group-averaged gene expression and receptor/transporter densities. To test this hypothesis, we used each gene's differential stability, a measure of gene expression variability across the six donors (see *Methods* for details (Hawrylycz et al., 2015)). Fig. 4a reveals that genes with greater differential stability, and therefore less inter-subject variance, are more correlated with PET-derived receptor density (Spearman $r = 0.84$, $p = 1.9 \times 10^{-6}$; for results in the subcortex, see Fig. S5). When we repeat the analyses in the autoradiography dataset, we find a similar trend (Spearman $r = 0.62$, $p = .003$; Fig. 4b). This suggests that receptor expression-density correlations are related to inter-subject variability. This may be due to genetic or non-genetic population variance and/or measurement factors such as variations in signal-to-noise ratios among probes or excessively spatially homogeneous patterns of gene expression. Interestingly, there is a positive correlation between genetic differential stability and the correspondence between PET- and autoradiography-derived receptor densities, which may suggest that this result is more broadly related to population variance rather than only inter-subject genetic variability or methodological error (although note this analysis is limited to the six receptors with both PET and autoradiography measurements; Fig. S6).

A second reason that neurotransmitter receptors might demonstrate low expression-density correspondence is that the protein is expressed at the synapse, which may be far from the cell body where gene transcription occurs. In this case, we would not observe a close regional expression-density relationship, but might find that high protein density in a brain region can be predicted by high mRNA levels in structurally connected brain regions. To test this, we correlate regional receptor density with the average gene expression in structurally connected regions, weighted by the structural connection (Hansen et al., 2022; Shafiei et al., 2022b; 2020). We repeat this using both PET and autoradiography datasets and find that receptors that already show high expression-density correlations also show high correlations between regional receptor density and neighbouring gene expression (Fig. S7). However, these relationships are not significant when controlling for

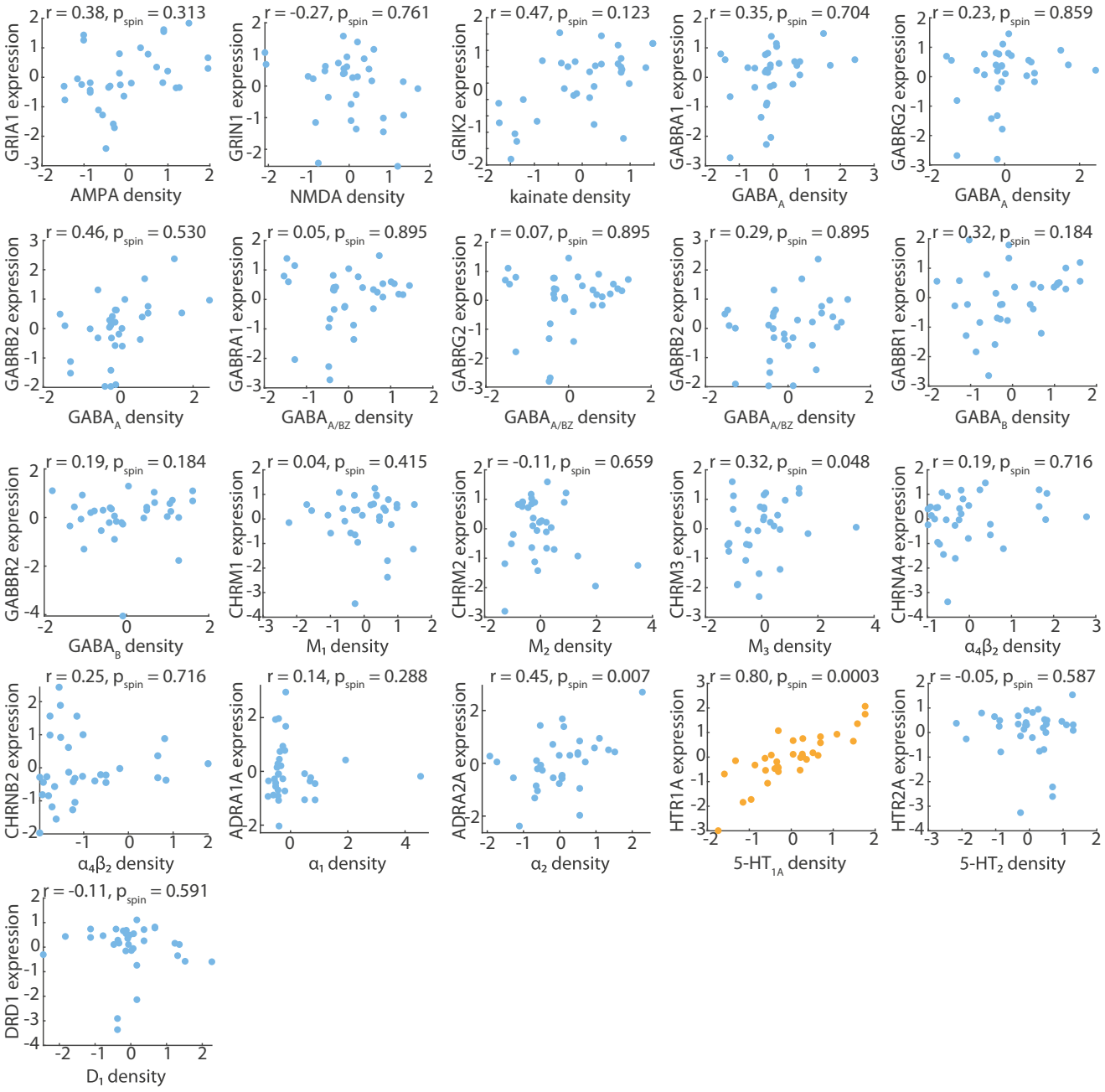

Fig. 2. Autoradiography-derived receptor densities versus gene expression | Autoradiographs for 15 different neurotransmitter receptors reveal that only 5-HT_{1A} and α_2 correlate significantly with the expression of their corresponding genes (*HTR1A* and *ADRA2A*, respectively), across 33 Desikan Killiany regions in the left cortex (Spearman r). Yellow scatter plots indicate significant ($p_{spin} < 0.05$) and large ($r > 0.5$) expression-density correspondence. Receptor density and gene expression is z-scored.

spatial autocorrelation. In other words, we do not find evidence that mRNA levels in neighbouring brain regions relate to protein density. One exception is the acetylcholine transporter, VAChT, which shows an improved, and significant, correlation between regional transporter density and neighbouring gene expression ($r = 0.46$, $p_{spin} = 0.04$, previously $r = 0.15$, $p_{spin} = 0.20$).

Extending the analysis from single genes to pathways

We conduct a final analysis that asks whether other genes in a biochemical pathway may be better predictors of receptor density than the receptor-coding gene itself. To test this, we use the Panther classification system (https://pantherdb.org/) to extract lists of genes coding for receptors within a protein pathway (Mi et al., 2012; Patania et al., 2019). Specifically, to maximize the number of genes, we search for each neurotransmitter name (e.g. "dopamine") and correlate each receptor within the neurotransmitter class (e.g. D_1 and D_2 receptors under "dopamine") with each gene in this list. We show our results in Table S6: broadly, after apply spin tests and FDR correction, we find that in most cases, receptors with poor expression-density correspondence do not show consistent improvement in expression-density correlation with other genes in the neurotransmitter pathway. Indeed, alternative significantly correlated genes only appear for receptors that already show high expression-density correlation (e.g. MOR, CB_1, 5-HT_{1A}, 5-HT_4), and these alternatives can be non-specific (e.g. *GNB2*, a gene coding for a G-protein subunit, is significantly correlated with both CB_1 and MOR density). This

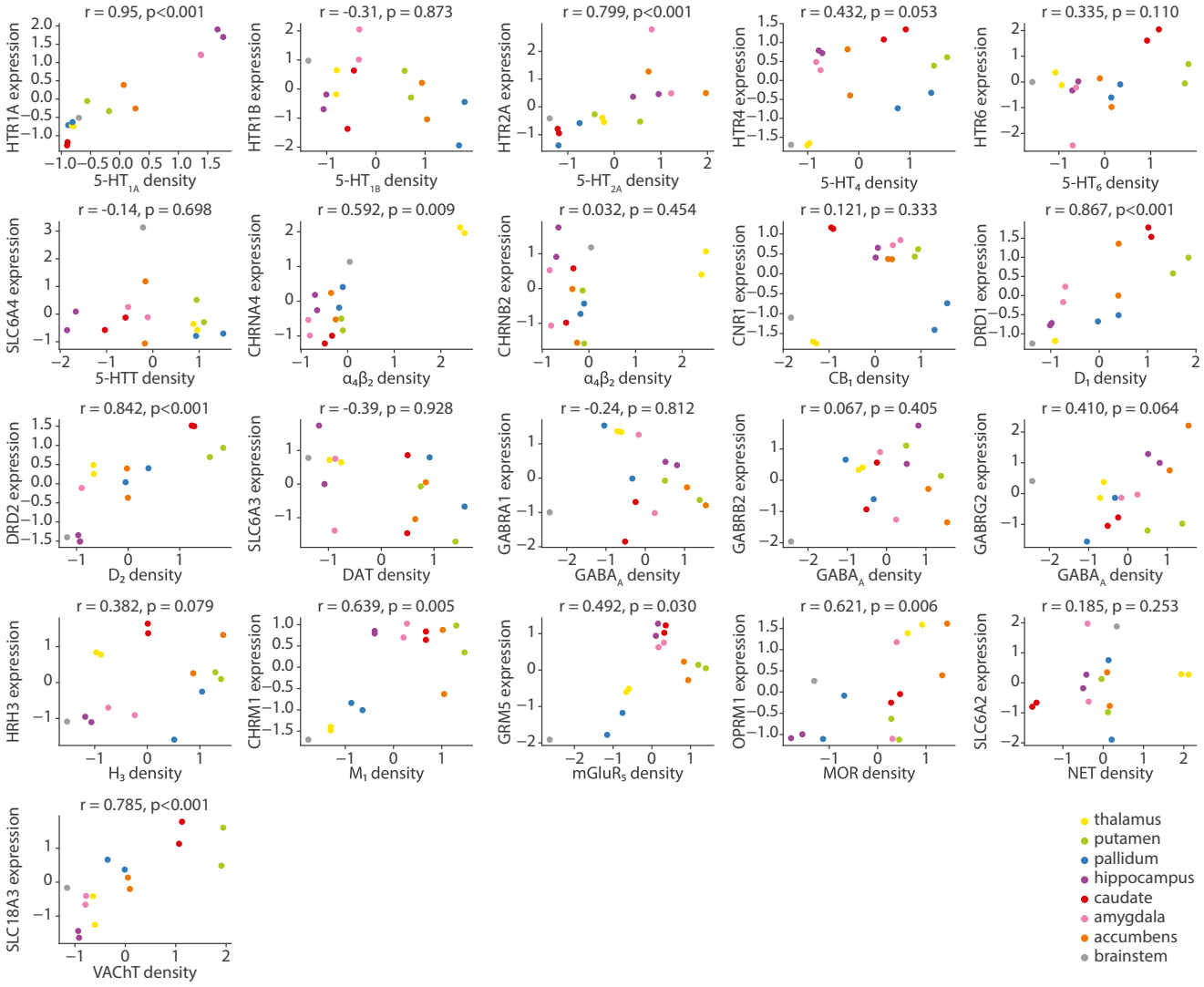

Fig. 3. Correspondence between gene expression and receptor/transporter density in the subcortex | PET receptor/transporter densities and microarray gene expression were parcellated into 15 subcortical regions and correlated. Points represent brain regions and are coloured by subcortical structure.

analysis can be extended in future work by taking a multivariate approach, or by using more specific search terms.

3. Discussion

Understanding how the chemoarchitecture of the brain modulates the link between structure and function requires accurate and comprehensive regional neurotransmitter receptor and transporter profiles. Here we formally test whether there is a correlation between gene expression and neurotransmitter receptor/transporter density, for a total of 27 unique neurotransmitter receptors, receptor binding sites, and transporters, from both PET images and autoradiographs. We find that only four receptors (5-HT_{1A}, CB_1, D_2, and MOR) display a robust close spatial correspondence between gene expression levels and receptor densities. We therefore conclude that researchers should exercise caution when using gene expression as a proxy for receptor and transporter densities.

We note that the lack of correlation between protein levels and the levels of their coding mRNA is not unreasonable as there are many mechanisms that may affect the protein-mRNA correlation. First, levels of mRNA detected on the AHBA microarray do not take into account the transcript isoforms that can be produced from the same gene, nor the stability of the resulting mRNA, which are determined by mRNA modifications such as splicing (Liu et al., 2016; Wang et al., 2009). Second, the proportion of different cell types in a microarray sample may distort the gene expression-protein density correspondence due to differences in the proteome and transcriptome, including different splice variant expression (Sharma et al., 2015; Zhang et al., 2014). Third, studies in bacteria (Li et al., 2014) and mice (Jovanovic et al., 2015) have demonstrated that rate of protein synthesis also alters protein levels. Fourth, protein buffering dampens the effect of variations in gene expression levels, including an adaptation of protein turnover through protein degradation, and the modulated activity of protein transport machinery which determines the final subcellular localization of the protein (Battle et al., 2015; Liu et al., 2016; Serdiuk et al., 2019; Yudowski et al., 2006). Fifth, the protein itself may be transported far from the coding mRNA, resulting in a spatial discrepancy between mRNA and protein levels. For example, the serotonin transporter 5-HTT is predominantly expressed on neurons innervating the cortex and therefore the majority of the associated mRNA transcripts are found in the subcortical cell bodies (Beliveau et al., 2017; Hoffman et al., 1998; Zhou et al., 1998). Altogether, the variation in the activity of these processes may contribute to the observed difference in levels of mRNA expression and protein abundance of receptors/transporters in the cortex.

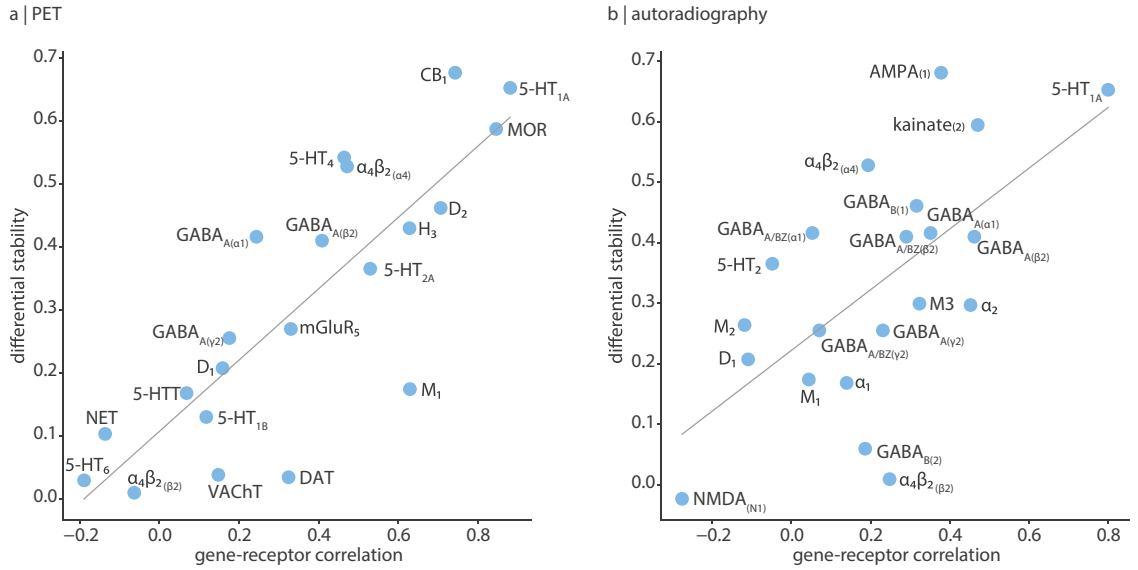

Fig. 4. Differentially stable genes are more correlated with neurotransmitter receptor density | We find that differential stability, a measure of the variability of a gene's expression across donors, is significantly correlated with gene-receptor Spearman correlations when using (a) PET-derived receptor/transporter densities (Spearman $r = 0.84$, $p = 1.9 \times 10^{-6}$) and (b) autoradiography-derived receptor densities (Spearman $r = 0.62$, $p = .003$). Labels are neurotransmitter receptors/transporters, and suffixes in parentheses refer to the receptor subunit, when relevant.

Furthermore, the regulatory mechanisms between gene transcription and protein expression at the cell surface are not necessarily conserved over the lifespan. In the present report, we are unable to thoroughly test the effects of age because each dataset—although spanning multiple neurotransmitter systems—includes participants of varying ages. This may contribute to the low correspondence between gene expression and receptor density. Indeed, some receptors have been shown to either increase (Cuypers et al., 2021) or decrease (Karrer et al., 2019) in density with healthy aging. This may be due to general changes in gene expression (in which case we would expect high expression-density correspondence throughout the lifespan, despite changes in receptor abundance), or due to changes in the regulatory mechanisms that govern the pathway between gene transcription and protein expression. How the link between gene expression and receptor density changes over the lifespan in both health and disease remains an exciting future research direction.

Nonetheless, we do find a small subset of neurotransmitter receptors that demonstrate close gene transcription-receptor density relationships. One possible explanation is rooted in inter-subject variability of gene expression and receptor densities. Since both receptor densities and gene expression are averaged across participants, genes and receptors with low inter-subject variability across the population would be better captured by the group-averaged map used in the present analyses. This is supported by the fact that neurotransmitter receptor densities are more correlated with genes that are more stable across donors (Fig. 4). Interestingly, we find evidence that genetic differential stability might also reflect the generalizability of receptor density measurements (Fig. S6b). The receptors and genes that show low genetic differential stability could inform future subject-level studies that focus on individual differences. Alternatively, expression-density correlations could be driven by the signal-to-noise ratio in the microarray data, or by how spatially homogeneous a gene's expression is across the cortex (which, assuming the presence of random noise, would result in low gene expression correspondence across donor brains even if the signal-to-noise ratio is high). This is another reason that we recommend researchers exercise caution when using receptor gene expression, especially if the gene's differential stability is low.

A second nonexclusive explanation is that the steps between gene transcription and membrane insertion are potentially more preserved for specific neurotransmitter receptors. Indeed, the correspondence between gene expression and receptor density would depend on localization of the mRNA due to differences in ribosome and tRNA availability (Besse and Ephrussi, 2008), as well as protein turnover rates at the location the receptor is expressed (Boisvert et al., 2012). Additionally, receptor systems that are phylogenetically older, involved in functions that require rigid stimulus-response relationships, or more fundamental to the organizational principles of the brain, may demonstrate more robust translation that manifest as close expression-density associations. For example, in the mouse cortex, gene expression for certain interneuron cell types are closely aligned with gradients of cortical organization (Fulcher et al., 2019). Interestingly, the gene that most recapitulates this organizational feature (*Pvalb*) is highly correlated to its corresponding protein's density (parvalbumin; Spearman $r = 0.95$), whereas *Sst*—an interneuron marker that is poorly aligned with cortical organization—is poorly correlated with somatostatin density (Spearman $r = 0.24$, $p = .1$) (Fulcher, 2019).

Altogether, the lack of expression-density correspondence reported here may be due to underlying biological mechanisms as well as technological limitations in measuring gene expression and receptor density. The question of how receptor gene expression and protein density relate will hopefully motivate further technological innovation to allow more spatially and biochemically precise measurements. For example, we observe an improvement in expression-density correlations in the finer parcellation for $mGluR_5$ and $5\text{-}HT_4$, suggesting that closer correspondences may be discovered with more spatially specific measurements. Furthermore, we observe higher subcortical correlations for D_1 and VAChT, opening the possibility that expression-density associations are spatially heterogeneous. More precise measurements would make it possible to test whether and how expression-density associations vary across the cortex. Future studies should measure RNA levels using single-cell or single-nucleus sequencing, and compare this to layer-specific autoradiography-derived receptor densities. Ideally, future studies will sample gene expression and receptor density in the same participants, making it possible to account for the effects of inter-individual variability on expression-density correspondence.

Importantly, the reported results are limited to the set of 27 proteins that we studied here. These results should not be extrapolated to other protein classes and do not preclude exciting work that uses

AHBA-derived microarray gene expression as a proxy for density of proteins involved in other functions such as metabolism, cellular signaling, or synapse formation (Medel et al., 2022; Shafiei et al., 2022a). Continued validation with open-source protein density datasets is necessary and increasingly possible thanks to emerging data sharing infrastructures and standards (Dukart et al., 2021; Hansen et al., 2021; Martins et al., 2021; Norgaard et al., 2022; Zilles and Palomero-Gallagher, 2017). Furthermore, both PET and autoradiography have specific challenges. For example, PET does not usually directly measure density, is sensitive to in-scanner motion, and some tracers may demonstrate non-specific binding (Ekelund et al., 2007). Meanwhile, autoradiographs more directly measure receptor densities but are only acquired post-mortem and in discrete brain sections (Zilles et al., 2002b). The fact that PET and autoradiography capture different features of chemoarchitecture is highlighted by how PET- and autoradiography-derived receptor density quantification are not always consistent. Of the receptors with measurements from both data modalities, we find that 5-HT_{1A} and $\alpha_4\beta_2$ are consistent but that D_1, $GABA_A$, 5-HT_2, and M_1 show poor consistency (Fig. S6a; although note that Beliveau et al. (2017) find a correlation between mRNA and autoradiography-derived 5-HT_2 densities). Indeed, there is a close relationship between mRNA and PET-derived M_1 density but no correspondence between mRNA levels or PET-derived M_1 density and autoradiography-derived density, which may indicate that, in this case, the mRNA measurement is more accurate than the autoradiography measurement. Interestingly, 5-HT_{1A} and $GABA_A$ show moderate to high expression-density correlations, suggesting that the consistency of density quantification across data modalities may be due to low inter-subject variance or fewer gene and protein modifications (Fig. S6b). These results demonstrate the value of using complementary techniques such as PET and autoradiography, but future efforts are needed to develop more accurate measures of protein density.

An alternative approach might be to test whether non receptor-coding genes serve as better predictors for receptor density. Since receptors act within biochemical pathways, it is possible that other mRNA transcripts for proteins within the pathway serve as better predictors than the receptor-coding gene, especially if the low expression-density correspondence is the product of genetic intersubject variability or measurement error. Indeed, gene expression from multiple genes is being increasingly used to infer biological pathways between transcription and neuroimaging markers (Martins et al., 2021; Romero-Garcia et al., 2018). A potential follow-up to this study would be to test the correspondence between receptor density and gene expression of proteins within the neurotransmitter pathway. This study would not be limited to the univariate expression-density correlation, but could consider combinations of genes in a multivariate analysis. Although direct protein quantification would be ideal, properly validated gene expression can serve as a viable alternative when protein density measurements are imprecise or unavailable.

Our results build on previous work that explores the expression-density relationship of specific neurotransmitter systems or receptors, such as the serotonergic system (Beliveau et al., 2017; Komorowski et al., 2017), the $GABA_A$ receptor (Nørgaard et al., 2021), and the opioid system (Komorowski et al., 2017; Rizzo et al., 2014), using PET and/or autoradiography-derived density. The present report comprehensively investigates the expression-density correspondence for 27 unique neurotransmitter receptors, receptor binding sites, and transporters across 9 different neurotransmitter systems using both PET and autoradiography measurements. Here we note some consistencies and inconsistencies across findings. Consistencies include: (1) high correlation between 5-HT_{1A} density and *HTR1A* expression (Beliveau et al., 2017; Komorowski et al., 2017; Rizzo et al., 2014), (2) weaker associations for other serotonergic receptors (Beliveau et al., 2017), (3) high correlation between MOR and *OPRM*$_1$ (Komorowski et al., 2017), and (4) positive correlation between $GABA_A$ density and β_2 subunit expression, but negative correlation between $GABA_A$ density and γ_1 subunit expression—although we do not find that these relationships are significant after correcting for multiple comparisons (Nørgaard et al., 2021). On the other hand, we find no association between $GABA_A$ density and the expression of α_1 and γ_2 main channel subunits, unlike that reported in Nørgaard et al. (2021). Additionally, Rizzo et al. (2014) find that the PET tracer dipenorphine, which binds to all three opioid subtypes (δ, κ, and μ), is not correlated with the expression of any opioid subtype. Meanwhile, we find a strong correlation between MOR density and *OPRM1* expression, and presume that expression-density relationships are specific to single receptors and not generalizable across receptors in the same neurotransmitter system. We note that these inconsistencies are likely related to the gene normalization method, a key processing step with large effects on estimated gene expression (Markello et al., 2021).

We close with some methodological considerations when working with PET, autoradiography, and gene expression datasets. First, our conclusions are limited to the scope of each dataset and should not be interpreted as a general rule-of-thumb that PET/autoradiography density measurements predict protein abundance better than microarray/RNAseq gene transcription. Second, gene expression estimates are derived from only six post-mortem human brains. Although the Allen Human Brain Atlas is a state-of-the-art dataset of microarray gene expression, more comprehensive datasets are necessary to confirm gene expression levels. Similarly, autoradiography data were collected for only three individuals, which inhibits population-level inferences. Third, measures of neurotransmitter receptor/transporter densities and gene expression are acquired in different individuals, so we are not able to make conclusions on the correspondence between gene expression and receptor/transporter density in the same cell tissue. Fourth, gene expression and receptor data were collected in participants of varying ages, but effects of age and sex could not be tested. Fifth, due to the relatively coarser resolution of PET, and the incomplete spatial coverage of autoradiography, main analyses were conducted in a parcellation of only 33–34 left hemisphere cortical brain regions. Replication in a finer parcellation for the PET receptor data do show similar results (Fig. S4), as well as high receptor density correlation between hemispheres, but high resolution whole-brain gene-receptor/transporter analyses should be conducted in future work.

In summary, we find that the expression of specific receptor/transporter-coding genes can generally not be used to estimate neurotransmitter receptor and transporter density. We only find a reliable correspondence between gene expression and receptor density for 5-HT_{1A}, CB_1, D_2, and MOR. Future efforts to map neurotransmitter receptor and transporter profiles to brain structure and function should verify the expression-density association when using microarray gene expression in place of receptor and transporter density.

4. Methods

Data and code availability

All code and data used to perform the analyses can be found at https://github.com/netneurolab/hansen_gene-receptor. The Allen Human Brain Atlas is available at https://human.brain-map.org/ (Hawrylycz et al., 2012). Volumetric PET receptor images can be found on `neuromaps` (https://netneurolab.github.io/neuromaps/ (Markello et al., 2022)) and at https://github.com/netneurolab/hansen_receptors (Hansen et al., 2021). Autoradiography receptor densities can be found in Supplementary Table 2 of Zilles and Palomero-Gallagher (2017). Structural connectivity data is collected from the Human Connectome Project, available at https://db.humanconnectome.org/.

PET data acquisition

Volumetric PET images were collected for 18 different neurotransmitter receptors and transporters across 9 different neurotransmitter

systems (Aghourian et al., 2017; Bedard et al., 2019; Beliveau et al., 2017; Ding et al., 2010; DuBois et al., 2016; Dukart et al., 2018; Gallezot et al., 2010; Hillmer et al., 2016; Kaller et al., 2017; Kantonen et al., 2020; Naganawa et al., 2021; Nørgaard et al., 2021; Normandin et al., 2015; Parker et al., 2015; Sandiego et al., 2015; Savli et al., 2012; Smart et al., 2019). To protect patient confidentiality, individual participant maps were averaged within studies before being shared. Each study, the associated receptor/transporter, tracer, number of healthy participants, age, and reference with full methodological details can be found in Table S1. In all cases, only scans from healthy participants were included. Images were acquired using best practice imaging protocols recommended for each radioligand. Altogether, the images are an estimate of receptor densities and we therefore refer to the measured value (i.e. binding potential, tracer distribution volume) simply as density. PET images were all registered to the MNI-ICBM 152 nonlinear 2009 (version c, asymmetric) template, then parcellated to a parcellation with 68 and 219 cortical regions, as well as 15 subcortical regions, according to the Lausanne atlas (Cammoun et al., 2012; Desikan et al., 2006). Receptors and transporters with more than one mean image of the same tracer (i.e. 5-HT_{1B}, D_2, $mGluR_5$, and VAChT) were averaged together in a manner that weights each image by the number of participants in the cohort. Tracer images are highly consistent across cohorts (see Fig. S1 in Hansen et al. (2021)). In some cases, images of multiple tracers for the same receptor were available. In these cases, we show the tracer with the larger number of participants in the main text, but we find consistent results when analyses are repeated for alternative tracers (Fig. S9). Finally, each tracer map corresponding to each receptor/transporter was z-scored across regions and concatenated into a final region×receptor matrix of relative densities. This data was presented and used originally in Hansen et al. (2021) and is available in `neuromaps` (https://netneurolab.github.io/neuromaps/) (Markello et al., 2022).

Autoradiography data acquisition

In vitro receptor autoradiography data were originally collected and processed as described in Zilles and Palomero-Gallagher (2017). Fifteen neurotransmitter receptor densities across 44 cytoarchitectonically identified areas in three post-mortem brains were acquired from Supplementary Table 2 of Zilles and Palomero-Gallagher (2017) (see Table S2 for a complete list of receptors included in the autoradiography dataset). Detailed information concerning the standard incubation protocols established over the last 25 years at Julich Research Centre and necessary for labeling the receptors is provided in Supplementary Table of Zilles and Palomero-Gallagher (2017) (see also Palomero-Gallagher and Zilles (2018); Zilles et al. (2002a,b)). Note that $GABA_A$ and $GABA_{A/BZ}$ refer to the same receptor, but that $GABA_{A/BZ}$ refers specifically to $GABA_A$ receptors containing the allosteric benzodiazepine binding site, as opposed to receptors containing only the GABA neurotransmitter binding site. To best compare PET data analyses with the autoradiography dataset, a region-to-region mapping was manually created between the 44 available cortical regions in the autoradiography dataset and the 34 left hemisphere cortical Desikan Killiany regions. In only one case (the insula) was there no suitable mapping between the autoradiography data and the Desikan Killiany atlas. As such, the 44-region autoradiography atlas was converted to 33 Desikan Killiany left hemisphere regions. Finally, receptor densities were z-scored and averaged across laminar layers, to create a single map of receptor densities across the cortex (for results across three laminar layers, see Fig. S2).

Microarray gene expression

Regional microarray expression data were obtained from six post-mortem brains provided by the Allen Human Brain Atlas (AHBA; http://human.brain-map.org/) (Hawrylycz et al., 2012). Since only two of the six brains included samples from the right hemisphere, main analyses were conducted on the left hemisphere only. All processing was performed using the *abagen* toolbox (https://github.com/netneurolab/abagen (Markello et al., 2021)). These data were processed and mapped to parcellated brain regions at 34 and 111 left hemisphere cortical grey matter nodes according to the Lausanne anatomical atlas (Cammoun et al., 2012; Desikan et al., 2006). For completeness, data were also parcellated to 15 bilateral subcortical regions. Due to the coarse subcortical parcellation, sufficient probes were available for both hemispheres.

Microarray probes were reannotated using data provided by Arnatkevičiūtė et al. (2019). A single microarray probe with the highest differential stability, $\Delta_S(p)$, was selected to represent each gene (Hawrylycz et al., 2015), where differential stability was calculated as:

$$\Delta_S(p) = \frac{1}{\binom{N}{2}} \sum_{i=1}^{N-1} \sum_{j=i+1}^{N} r[B_i(p), B_j(p)] \tag{1}$$

Here, r is Spearman's rank correlation of the expression of a single probe p across regions in two donor brains, B_i and B_j, and N is the total number of donor brains. Differential stability is the average correlation across every pair of donor brains of a probe's expression. This procedure retained 20 232 probes, each representing a unique gene. We repeat the analyses using alternative probe selection methods and find consistent results (Fig. S10).

Next, samples were assigned to brain regions using MNI coordinates generated via non-linear registrations (https://github.com/chrisfilo/alleninf) by finding the nearest region, up to 2 mm away. To reduce the potential for misassignment, sample-to-region matching was constrained by hemisphere and cortical/subcortical divisions (Arnatkevičiūtė et al., 2019). If a brain region was not assigned any sample based on the above procedure, the sample closest to the centroid of that region was selected in order to ensure that all brain regions were assigned a value.

Inter-subject variation was addressed by normalizing tissue sample expression values for each donor across genes using a scaled robust sigmoid function (Fulcher and Fornito, 2016):

$$x_{norm} = \frac{1}{1 + \exp(-\frac{(x_g - \langle x_g \rangle)}{\mathrm{IQR}_x})} \tag{2}$$

where $\langle x_g \rangle$ is the median and IQR is the normalized interquartile range of the expression value of a single gene across regions. Normalized gene expression values were then rescaled to a unit interval:

$$x_{scaled} = \frac{x_{norm} - \min(x_{norm})}{\max(x_{norm}) - \min(x_{norm})} \tag{3}$$

Gene expression values were normalized across tissue samples using the same procedure. Samples assigned to the same brain region were then averaged separately for each donor. Scaled regional expression profiles were finally averaged across donors.

Finally, we repeat all analyses using RNAseq data collected from the two donors with RNAseq measurements (see Fig. S1 and Fig. S3) (Hawrylycz et al., 2012). Gene expression-receptor density associations across neurotransmitter receptors in both the PET and autoradiography datasets remain consistent whether gene expression is derived from the microarray or RNAseq (Fig. S11).

Gene-receptor pairs

With the notable exception of the $GABA_B$ receptor, metabotropic neurotransmitter receptors are monomeric structures, and thus a single gene codes for the entire receptor. Therefore, the expression of the receptor-coding gene was correlated with the density of the receptor itself. The $GABA_B$ and ionotropic receptors are characterized by being multimeric protein complexes, so each receptor was correlated with microarray expression of all possible receptor subunits. Below, we outline each multimeric case.

- $GABA_A$ is a pentamer typically composed of three primary subunits (α_1, β_2, and γ_2) but can be built out of a total of nineteen different subunits. For simplicity, we show results for the three primary subunits in the main text, but results for the remaining sixteen subunits can be found in Fig. S12.
- $GABA_B$, a multimeric metabotropic receptor, is composed of two subunits. We show both in the main analyses.
- AMPA is a heterotetramer that typically consists of two pairs of duplicate subunits. These two pairs can be formed from any combination of four subunits. We show results for the gene whose expression is most highly correlated with AMPA density in the main text (*GRIA1*).
- NMDA is also a heterotetramer, typically composed of two *N1* and two *N2* subunits, although there are four different *N2*-encoding genes, as well as a third subunit (*N3*) for which there are two subunit-encoding genes. The main analyses use the expression of the *N1*-encoding gene (*GRIN1*).
- Kainate exists as both a homotetramer and heterotetramer, built from any of five subunits. We show results for the gene whose expression is most highly correlated with kainate density in the main text (*GRIK2*).
- $\alpha_4\beta_2$ is a pentamer typically composed of two α_4 subunits and three β_2 subunits (Dani, 2015). However, the ligand used for the autoradiograph, epibatidin, binds to any heteromeric nicotinic receptors that contain both an alpha subunit (α_2–α_7, α_9, α_{10}) and a beta subunit (β_2–β_4). The most abundant such receptor in the brain is the $\alpha_4\beta_2$ receptor, so we focus on gene expression of the α_4 and β_2 subunits (*CHRNA4* and *CHRNB2*, respectively) in the main text.

Correlations between neurotransmitter receptor density and multiple subunit expression were corrected for multiple comparisons using the Benjamini-Hochberg FDR correction (Benjamini and Hochberg, 1995). Correlation coefficients and corrected *p*-values (see *Null model*) for all subunits can be found in Table S3 (PET, cortex) Table S4 (PET, subcortex), and Table S5 (autoradiography) as well as in stand-alone machine-readable supplementary csv files.

Null model

Spatial autocorrelation-preserving permutation tests were used to assess statistical significance of associations across brain regions, termed "spin tests" (Alexander-Bloch et al., 2018; Markello and Misic, 2021). Parametric *p*-values were not used because spatially embedded systems such as the brain violate the assumption that observations (brain regions) are independent from one another. We created a surface-based representation of the parcellation on the FreeSurfer fsaverage left hemisphere surface, via files from the Connectome Mapper toolkit (https://github.com/LTS5/cmp). We used the spherical projection of the fsaverage left hemisphere surface to define spatial coordinates for each parcel by selecting the coordinates of the vertex closest to the center of the mass of each parcel (Vázquez-Rodríguez et al., 2019). These parcel coordinates were then randomly rotated, and original parcels were reassigned the value of the closest rotated parcel (10 000 repetitions). Parcels for which the medial wall was closest were assigned the value of the next most proximal parcel instead. The procedure was performed at the parcel resolution rather than the vertex resolution to avoid upsampling the data, and only to the left hemisphere. In the autoradiography dataset, null correlations were computed ignoring the insula and regions resampled to the insula, for a maximum of three ignored brain regions. All reported *p*-values for expression-density correlations are one-tailed.

Structural connectivity

Following the procedure described in de Wael et al. (2018), we obtained diffusion weighted imaging data for 326 unrelated participants (age range 2235 years, 145 males) from the Human Connectome Project (HCP; S900 release (Van Essen et al., 2013)). DWI data was pre-processed using the MRtrix3 package (Tournier et al., 2019) (https://www.mrtrix.org/). More specifically, fiber orientation distributions were generated using the multi-shell multi-tissue constrained spherical deconvolution algorithm from MRtrix (Dhollander et al., 2016; Jeurissen et al., 2014). White matter edges were then reconstructed using probabilistic streamline tractography based on the generated fiber orientation distributions (Tournier et al., 2010). The tract weights were then optimized by estimating an appropriate cross-section multiplier for each streamline following the procedure proposed by Smith et al. (2015) and a connectivity matrix was built for each participant using the 68-region Deskian-Killiany parcellation (Cammoun et al., 2012; Desikan et al., 2006). Collating each individual's structural connectome was done using a group-consensus approach that seeks to preserve the density and edge-length distributions of the individual connectomes (Betzel et al., 2019). The binary density for the final whole-brain structural connectome was 31.2%. Edges were weighted by the average log-transform of non-zero streamline density, scaled to values between 0 and 1. Detailed information regarding data acquisition and pre-processing is also available elsewhere (Glasser et al., 2013; Van Essen et al., 2013).

Competing interests

RDM is currently employed by Octave Bioscience. The work contributing to the manuscript was performed as part of his graduate studies at McGill University, and is in no way related to his employment at Octave Bioscience. The remaining authors declare no competing interests.

Credit authorship contribution statement

Justine Y. Hansen: Conceptualization, Formal analysis, Investigation, Methodology, Software, Visualization, Writing – original draft, Writing – review & editing. **Ross D. Markello:** Methodology, Resources, Writing – review & editing. **Lauri Tuominen:** Resources, Data curation, Investigation, Writing – review & editing. **Martin Nørgaard:** Resources, Data curation, Investigation, Writing – review & editing. **Elena Kuzmin:** Writing – review & editing. **Nicola Palomero-Gallagher:** Resources, Data curation, Investigation, Writing – review & editing. **Alain Dagher:** Conceptualization, Writing – review & editing. **Bratislav Misic:** Conceptualization, Funding acquisition, Methodology, Project administration, Supervision, Writing – original draft, Writing – review & editing.

Acknowledgments

We thank Kelly Smart, Sylvia Cox, Yanjun Wu, Jean-Dominique Gallezot, Étienne Aumont, Stijn Servaes, Stephanie G. Scala, Jonathan M. DuBois, Gleb Bezgin, Taylor W. Schmitz, R. Nathan Spreng, Jean-Paul Soucy, Synthia Guimond, Jarmo Hietala, Marc-André Bédard, Marco Leyton, Eliane Kobayashi, Pedro Rosa-Neto, and Richard E. Carson for collecting and sharing the PET data presented here. We thank Golia Shafiei, Vincent Bazinet, Zhen-Qi Liu, Filip Milisav, Laura Suarez, and Mingze Li for their comments and suggestions on the manuscript. This research was undertaken thanks in part to funding from the Canada First Research Excellence Fund, awarded to McGill University for the Healthy Brains for Healthy Lives initiative. BM acknowledges support from the Natural Sciences and Engineering Research Council of Canada (NSERC Discovery Grant RGPIN #017-04265) and from the Canada Research Chairs Program. JYH acknowledges support from the Helmholtz International BigBrain Analytics & Learning Laboratory, the Natural Sciences and Engineering Research Council of Canada, and the Fonds de reserches de Québec. MN was supported by the Independent Research Fund Denmark (DFF-0129-00004B). The funders had no role in study design, data collection and analysis, decision to publish or preparation of the manuscript.

Supplementary material

Supplementary material associated with this article can be found, in the online version, at 10.1016/j.neuroimage.2022.119671

References

Aghourian, M., Legault-Denis, C., Soucy, J., Rosa-Neto, P., Gauthier, S., Kostikov, A., Gravel, P., Bedard, M., 2017. Quantification of brain cholinergic denervation in alzheimer's disease using pet imaging with [18 f]-feobv. Mol. Psychiatry 22 (11), 1531–1538.

Alexander-Bloch, A.F., Shou, H., Liu, S., Satterthwaite, T.D., Glahn, D.C., Shinohara, R.T., Vandekar, S.N., Raznahan, A., 2018. On testing for spatial correspondence between maps of human brain structure and function. Neuroimage 178, 540–551.

Arnatkevičiūtė, A., Fulcher, B.D., Fornito, A., 2019. A practical guide to linking brain-wide gene expression and neuroimaging data. Neuroimage 189, 353–367.

Ballentine, G., Friedman, S.F., Bzdok, D., 2021. Trips and neurotransmitters: discovering principled patterns across 6,850 hallucinogenic experiences. bioRxiv.

Battle, A., Khan, Z., Wang, S.H., Mitrano, A., Ford, M.J., Pritchard, J.K., Gilad, Y., 2015. Impact of regulatory variation from rna to protein. Science 347 (6222), 664–667.

Bedard, M.-A., Aghourian, M., Legault-Denis, C., Postuma, R.B., Soucy, J.-P., Gagnon, J.-F., Pelletier, A., Montplaisir, J., 2019. Brain cholinergic alterations in idiopathic rem sleep behaviour disorder: a pet imaging study with 18f-feobv. Sleep Med. 58, 35–41.

Beliveau, V., Ganz, M., Feng, L., Ozenne, B., Højgaard, L., Fisher, P.M., Svarer, C., Greve, D.N., Knudsen, G.M., 2017. A high-resolution in vivo atlas of the human brain's serotonin system. J. Neurosci. 37 (1), 120–128.

Benjamini, Y., Hochberg, Y., 1995. Controlling the false discovery rate: a practical and powerful approach to multiple testing. J. R. Stat. Soc. B. 57 (1), 289–300.

Besse, F., Ephrussi, A., 2008. Translational control of localized mrnas: restricting protein synthesis in space and time. Nat. Rev. Mol. Cell Biol. 9 (12), 971–980.

Betzel, R.F., Griffa, A., Hagmann, P., Mišić, B., 2019. Distance-dependent consensus thresholds for generating group-representative structural brain networks. Netw. Neurosci. 3 (2), 475–496.

Boisvert, F.-M., Ahmad, Y., Gierliński, M., Charrière, F., Lamont, D., Scott, M., Barton, G., Lamond, A.I., 2012. A quantitative spatial proteomics analysis of proteome turnover in human cells. Mol. Cell. Proteomic. 11 (3).

Braun, U., Harneit, A., Pergola, G., Menara, T., Schäfer, A., Betzel, R.F., Zang, Z., Schweiger, J.I., Zhang, X., Schwarz, K., et al., 2021. Brain network dynamics during working memory are modulated by dopamine and diminished in schizophrenia. Nat. Commun. 12 (1), 1–11.

Burt, J.B., Demirtaş, M., Eckner, W.J., Navejar, N.M., Ji, J.L., Martin, W.J., Bernacchia, A., Anticevic, A., Murray, J.D., 2018. Hierarchy of transcriptomic specialization across human cortex captured by structural neuroimaging topography. Nat. Neurosci. 21 (9), 1251–1259.

Burt, J.B., Preller, K.H., Demirtas, M., Ji, J.L., Krystal, J.H., Vollenweider, F.X., Anticevic, A., Murray, J.D., 2021. Transcriptomics-informed large-scale cortical model captures topography of pharmacological neuroimaging effects of lsd. bioRxiv.

Cammoun, L., Gigandet, X., Meskaldji, D., Thiran, J.P., Sporns, O., Do, K.Q., Maeder, P., Meuli, R., Hagmann, P., 2012. Mapping the human connectome at multiple scales with diffusion spectrum mri. J. Neurosci. Meth. 203 (2), 386–397.

Chang, T.-H., Gloria, Y.C., Hellmann, M.J., Greve, C.L., Le Roy, D., Roger, T., Kasper, L., Hube, B., Pusch, S., Gow, N., et al., 2022. Transkingdom mechanism of mamp generation by chitotriosidase (chit1) feeds oligomeric chitin from fungal pathogens and allergens into tlr2-mediated innate immune sensing. bioRxiv.

Cuypers, K., Hehl, M., van Aalst, J., Chalavi, S., Mikkelsen, M., Van Laere, K., Dupont, P., Mantini, D., Swinnen, S.P., 2021. Age-related gabaergic differences in the primary sensorimotor cortex: a multimodal approach combining pet, mrs and tms. Neuroimage 226, 117536.

Dagher, A., Palomero-Gallagher, N., 2020. Mapping dopamine with positron emission tomography: anote of caution. Neuroimage 207, 116203.

Dani, J.A., 2015. Neuronal nicotinic acetylcholine receptor structure and function and response to nicotine. Int. Rev. Neurobiol. 124, 3–19.

Deco, G., Aquino, K.M., Arnatkeviciute, A., Oldham, S., Sabaroedin, K., Rogasch, N.C., Kringelbach, M.L., Fornito, A., 2020. Dynamical consequences of regional heterogeneity in the brains transcriptional landscape. bioRxiv.

Desikan, R.S., Ségonne, F., Fischl, B., Quinn, B.T., Dickerson, B.C., Blacker, D., Buckner, R.L., Dale, A.M., Maguire, R.P., Hyman, B.T., et al., 2006. An automated labeling system for subdividing the human cerebral cortex on mri scans into gyral based regions of interest. Neuroimage 31 (3), 968–980.

Dhollander, T., Raffelt, D., Connelly, A., 2016. Unsupervised 3-tissue response function estimation from single-shell or multi-shell diffusion mr data without a co-registered t1 image. ISMRM Workshop on Breaking the Barriers of Diffusion MRI, Vol. 5. ISMRM.

Ding, Y.-S., Singhal, T., Planeta-Wilson, B., Gallezot, J.-D., Nabulsi, N., Labaree, D., Ropchan, J., Henry, S., Williams, W., Carson, R.E., et al., 2010. Pet imaging of the effects of age and cocaine on the norepinephrine transporter in the human brain using (s, s)-[11c] o-methylreboxetine and hrrt. Synapse 64 (1), 30–38.

DuBois, J.M., Rousset, O.G., Rowley, J., Porras-Betancourt, M., Reader, A.J., Labbe, A., Massarweh, G., Soucy, J.-P., Rosa-Neto, P., Kobayashi, E., 2016. Characterization of age/sex and the regional distribution of mglur5 availability in the healthy human brain measured by high-resolution [11 c] abp688 pet. Eur. J. Nucl. Med. Mol. Imaging 43 (1), 152–162.

Dukart, J., Holiga, Š., Chatham, C., Hawkins, P., Forsyth, A., McMillan, R., Myers, J., Lingford-Hughes, A.R., Nutt, D.J., Merlo-Pich, E., et al., 2018. Cerebral blood flow predicts differential neurotransmitter activity. Sci. Rep. 8 (1), 1–11.

Dukart, J., Holiga, S., Rullmann, M., Lanzenberger, R., Hawkins, P.C., Mehta, M.A., Hesse, S., Barthel, H., Sabri, O., Jech, R., et al., 2021. JuSpace: A tool for spatial correlation analyses of magnetic resonance imaging data with nuclear imaging derived neurotransmitter maps. Technical Report. Wiley Online Library.

Ekelund, J., Slifstein, M., Narendran, R., Guillin, O., Belani, H., Guo, N.-N., Hwang, Y., Hwang, D.-R., Abi-Dargham, A., Laruelle, M., 2007. In vivo da d 1 receptor selectivity of nnc 112 and sch 23390. Mol. Imag. Biol. 9 (3), 117–125.

Froudist-Walsh, S., Xu, T., Niu, M., Rapan, L., Zilles, K., Margulies, D.S., Wang, X.-J., Palomero-Gallagher, N., 2021. Gradients of receptor expression in the macaque cortex. bioRxiv.

Fulcher, B.D., 2019. Discovering conserved properties of brain organization through multimodal integration and interspecies comparison. J. Exp. Neurosci. 13 1179069519862047.

Fulcher, B.D., Fornito, A., 2016. A transcriptional signature of hub connectivity in the mouse connectome. Proc. Natl. Acad. Sci. USA 113 (5), 1435–1440.

Fulcher, B.D., Murray, J.D., Zerbi, V., Wang, X.-J., 2019. Multimodal gradients across mouse cortex. Proc. Natl. Acad. Sci. USA 116 (10), 4689–4695.

Gallezot, J.-D., Nabulsi, N., Neumeister, A., Planeta-Wilson, B., Williams, W.A., Singhal, T., Kim, S., Maguire, R.P., McCarthy, T., Frost, J.J., et al., 2010. Kinetic modeling of the serotonin 5-ht1b receptor radioligand [11c] p943 in humans. J. Cerebral Blood Flow Metabol. 30 (1), 196–210.

Gao, R., van den Brink, R.L., Pfeffer, T., Voytek, B., 2020. Neuronal timescales are functionally dynamic and shaped by cortical microarchitecture. Elife 9, e61277.

Glasser, M.F., Sotiropoulos, S.N., Wilson, J.A., Coalson, T.S., Fischl, B., Andersson, J.L., Xu, J., Jbabdi, S., Webster, M., Polimeni, J.R., et al., 2013. The minimal preprocessing pipelines for the human connectome project. Neuroimage 80, 105–124.

Goulas, A., Changeux, J.-P., Wagstyl, K., Amunts, K., Palomero-Gallagher, N., Hilgetag, C.C., 2021. The natural axis of transmitter receptor distribution in the human cerebral cortex. Proc. Natl. Acad. Sci. 118 (3).

Hansen, J.Y., Shafiei, G., Markello, R.D., Smart, K., Cox, S., Wu, Y., Gallezot, J.-D., Étienne, A., Servaes, S., Scala, S.G., DuBois, J.M., Wainstein, G., Bezgin, G., Funck, T., Schmitz, T.W., Spreng, R.N., Soucy, J.-P., Baillet, S., Guimond, S., Hietala, J., Bédard, M.-A., Leyton, M., Kobayashi, E., Rosa-Neto, P., Palomero-Gallagher, N., Shine, J.M., Carson, R.E., Tuominen, L., Dagher, A., Misic, B., 2021. Mapping neurotransmitter systems to the structural and functional organization of the human neocortex. bioRxiv.

Hansen, J.Y., Shafiei, G., Vogel, J.W., Smart, K., Bearden, C.E., Hoogman, M., Franke, B., Van Rooij, D., Buitelaar, J., McDonald, C.R., et al., 2022. Local molecular and global connectomic contributions to cross-disorder cortical abnormalities. Nat. Commun. 13 (1), 1–17.

Hawrylycz, M., Miller, J.A., Menon, V., Feng, D., Dolbeare, T., Guillozet-Bongaarts, A.L., Jegga, A.G., Aronow, B.J., Lee, C.-K., Bernard, A., et al., 2015. Canonical genetic signatures of the adult human brain. Nat. Neurosci. 18 (12), 1832.

Hawrylycz, M.J., Lein, E.S., Guillozet-Bongaarts, A.L., Shen, E.H., Ng, L., Miller, J.A., Van De Lagemaat, L.N., Smith, K.A., Ebbert, A., Riley, Z.L., et al., 2012. An anatomically comprehensive atlas of the adult human brain transcriptome. Nature 489 (7416), 391.

Hillmer, A.T., Esterlis, I., Gallezot, J.-D., Bois, F., Zheng, M.-Q., Nabulsi, N., Lin, S.-F., Papke, R., Huang, Y., Sabri, O., et al., 2016. Imaging of cerebral $\alpha 4\beta 2^*$ nicotinic acetylcholine receptors with (-)-[18f] flubatine pet: implementation of bolus plus constant infusion and sensitivity to acetylcholine in human brain. Neuroimage 141, 71–80.

Hoffman, B.J., Hansson, S.R., Mezey, E., Palkovits, M., 1998. Localization and dynamic regulation of biogenic amine transporters in the mammalian central nervous system. Front. Neuroendocrinol. 19 (3), 187–231.

Hoftman, G.D., Dienel, S.J., Bazmi, H.H., Zhang, Y., Chen, K., Lewis, D.A., 2018. Altered gradients of glutamate and gamma-aminobutyric acid transcripts in the cortical visuospatial working memory network in schizophrenia. Biol. Psychiatry 83 (8), 670–679.

Jeurissen, B., Tournier, J.-D., Dhollander, T., Connelly, A., Sijbers, J., 2014. Multi-tissue constrained spherical deconvolution for improved analysis of multi-shell diffusion mri data. Neuroimage 103, 411–426.

Jovanovic, M., Rooney, M.S., Mertins, P., Przybylski, D., Chevrier, N., Satija, R., Rodriguez, E.H., Fields, A.P., Schwartz, S., Raychowdhury, R., et al., 2015. Dynamic profiling of the protein life cycle in response to pathogens. Science 347 (6226).

Kaller, S., Rullmann, M., Patt, M., Becker, G.-A., Luthardt, J., Girbardt, J., Meyer, P.M., Werner, P., Barthel, H., Bresch, A., et al., 2017. Test–retest measurements of dopamine d 1-type receptors using simultaneous pet/mri imaging. Eur. J. Nucl. Med. Mol. Imaging 44 (6), 1025–1032.

Kantonen, T., Karjalainen, T., Isojärvi, J., Nuutila, P., Tuisku, J., Rinne, J., Hietala, J., Kaasinen, V., Kalliokoski, K., Scheinin, H., et al., 2020. Interindividual variability and lateralization of μ-opioid receptors in the human brain. Neuroimage 217, 116922.

Karrer, T.M., McLaughlin, C.L., Guaglianone, C.P., Samanez-Larkin, G.R., 2019. Reduced serotonin receptors and transporters in normal aging adults: a meta-analysis of pet and spect imaging studies. Neurobiol. Aging 80, 1–10.

Komorowski, A., James, G., Philippe, C., Gryglewski, G., Bauer, A., Hienert, M., Spies, M., Kautzky, A., Vanicek, T., Hahn, A., et al., 2017. Association of protein distribution and gene expression revealed by pet and post-mortem quantification in the serotonergic system of the human brain. Cereb. Cortex 27 (1), 117–130.

Larsen, B., Cui, Z., Adebimpe, A., Pines, A.R., Alexander-Bloch, A., Bertolero, M., Calkins, M.E., Gur, R.E., Gur, R.C., Mahadevan, A.S., et al., 2021. A developmental reduction of the excitation: inhibition ratio in association cortex during adolescence. bioRxiv.

Li, G.-W., Burkhardt, D., Gross, C., Weissman, J.S., 2014. Quantifying absolute protein synthesis rates reveals principles underlying allocation of cellular resources. Cell 157 (3), 624–635.

Liu, Y., Beyer, A., Aebersold, R., 2016. On the dependency of cellular protein levels on mrna abundance. Cell 165 (3), 535–550.

Markello, R.D., Arnatkeviciute, A., Poline, J.-B., Fulcher, B.D., Fornito, A., Misic, B., 2021. Standardizing workflows in imaging transcriptomics with the abagen toolbox. Elife 10, e72129.
Markello, R.D., Hansen, J.Y., Liu, Z.-Q., Bazinet, V., Shafiei, G., Suarez, L.E., Blostein, N., Seidlitz, J., Baillet, S., Satterthwaite, T.D., et al., 2022. Neuromaps: structural and functional interpretation of brain maps. bioRxiv.
Markello, R.D., Misic, B., 2021. Comparing spatial null models for brain maps. Neuroimage 118052.
Martins, D., Giacomel, A., Williams, S.C., Turkheimer, F., Dipasquale, O., Veronese, M., Group, P.T.W., et al., 2021. Imaging transcriptomics: convergent cellular, transcriptomic, and molecular neuroimaging signatures in the healthy adult human brain. Cell Rep. 37 (13), 110173.
Medel, V., Crossley, N., Gajardo, I., Muller, E., Barros, L.F., Shine, J.M., Sierralta, J., 2022. Whole-brain neuronal mct2 lactate transporter expression links metabolism to human brain structure and function. Proc. Natl. Acad. Sci. 119 (33) e2204619119.
Mi, H., Muruganujan, A., Thomas, P.D., 2012. Panther in 2013: modeling the evolution of gene function, and other gene attributes, in the context of phylogenetic trees. Nucleic Acids Res. 41 (D1), D377–D386.
Mühleisen, T., Zhao, L., Hilger, D., Burger, B., Forstner, A., Herms, S., Hoffmann, P., Zilles, K., Amunts, K., Cichon, S., Palomer-Gallagher, N., 2021. Comparison of transcript levels adn neurotransmitter receptor densities in human hippocampal regions. 27th Annual Meeting of the Organization for Human Brain Mapping..
Murgaš, M., Michenthaler, P., Reed, M.B., Gryglewski, G., Lanzenberger, R., 2022. Correlation of receptor density and mrna expression patterns in the human cerebral cortex. Neuroimage 256, 119214.
Naganawa, M., Nabulsi, N., Henry, S., Matuskey, D., Lin, S.-F., Slieker, L., Schwarz, A.J., Kant, N., Jesudason, C., Ruley, K., et al., 2021. First-in-human assessment of 11c-lsn3172176, an m1 muscarinic acetylcholine receptor pet radiotracer. J. Nucl. Med. 62 (4), 553–560.
Nørgaard, M., Beliveau, V., Ganz, M., Svarer, C., Pinborg, L.H., Keller, S.H., Jensen, P.S., Greve, D.N., Knudsen, G.M., 2021. A high-resolution in vivo atlas of the human brain's benzodiazepine binding site of gabaa receptors. Neuroimage 232, 117878.
Norgaard, M., Matheson, G.J., Hansen, H.D., Thomas, A., Searle, G., Rizzo, G., Veronese, M., Giacomel, A., Yaqub, M., Tonietto, M., et al., 2022. Pet-bids, an extension to the brain imaging data structure for positron emission tomography. Sci. Data 9 (1), 1–7.
Normandin, M.D., Zheng, M.-Q., Lin, K.-S., Mason, N.S., Lin, S.-F., Ropchan, J., Labaree, D., Henry, S., Williams, W.A., Carson, R.E., et al., 2015. Imaging the cannabinoid cb1 receptor in humans with [11c] omar: assessment of kinetic analysis methods, test–retest reproducibility, and gender differences. J. Cereb. Blood Flow Metabol. 35 (8), 1313–1322.
Palomero-Gallagher, N., Zilles, K., 2018. Cyto-and Receptor Architectonic Mapping of the Human Brain. In: Handbook of clinical neurology, Vol. 150. Elsevier, pp. 355–387.
Palomero-Gallagher, N., Zilles, K., 2019. Cortical layers: cyto-, myelo-, receptor-and synaptic architecture in human cortical areas. Neuroimage 197, 716–741.
Parker, C.A., Rabiner, E.A., Gunn, R.N., Searle, G., Martarello, L., Comley, R.A., Davy, M., Wilson, A.A., Houle, S., Mizrahi, R., et al., 2015. Human kinetic modeling of the 5ht6 pet radioligand 11c-gsk215083 and its utility for determining occupancy at both 5ht6 and 5ht2a receptors by sb742457 as a potential therapeutic mechanism of action in alzheimer disease. J. Nucl. Med. 56 (12), 1901–1909.
Patania, A., Selvaggi, P., Veronese, M., Dipasquale, O., Expert, P., Petri, G., 2019. Topological gene expression networks recapitulate brain anatomy and function. Netw. Neurosci. 3 (3), 744–762.
Preller, K.H., Burt, J.B., Ji, J.L., Schleifer, C.H., Adkinson, B.D., Stämpfli, P., Seifritz, E., Repovs, G., Krystal, J.H., Murray, J.D., et al., 2018. Changes in global and thalamic brain connectivity in lsd-induced altered states of consciousness are attributable to the 5-ht2a receptor. Elife 7, e35082.
Preller, K.H., Duerler, P., Burt, J.B., Ji, J.L., Adkinson, B., Stämpfli, P., Seifritz, E., Repovš, G., Krystal, J.H., Murray, J.D., et al., 2020. Psilocybin induces time-dependent changes in global functional connectivity. Biol. Psychiatry 88 (2), 197–207.
Rizzo, G., Veronese, M., Heckemann, R.A., Selvaraj, S., Howes, O.D., Hammers, A., Turkheimer, F.E., Bertoldo, A., 2014. The predictive power of brain mrna mappings for in vivo protein density: a positron emission tomography correlation study. J. Cereb. Blood Flow Metabol. 34 (5), 827–835.
Romero-Garcia, R., Whitaker, K.J., Váša, F., Seidlitz, J., Shinn, M., Fonagy, P., Dolan, R.J., Jones, P.B., Goodyer, I.M., Bullmore, E.T., et al., 2018. Structural covariance networks are coupled to expression of genes enriched in supragranular layers of the human cortex. Neuroimage 171, 256–267.
Sandiego, C.M., Gallezot, J.-D., Lim, K., Ropchan, J., Lin, S.-f., Gao, H., Morris, E.D., Cosgrove, K.P., 2015. Reference region modeling approaches for amphetamine challenge studies with [11c] flb 457 and pet. J. Cereb. Blood Flow Metabol. 35 (4), 623–629.
Savli, M., Bauer, A., Mitterhauser, M., Ding, Y.-S., Hahn, A., Kroll, T., Neumeister, A., Haeusler, D., Ungersboeck, J., Henry, S., et al., 2012. Normative database of the serotonergic system in healthy subjects using multi-tracer pet. Neuroimage 63 (1), 447–459.
Schwanhäusser, B., Busse, D., Li, N., Dittmar, G., Schuchhardt, J., Wolf, J., Chen, W., Selbach, M., 2011. Global quantification of mammalian gene expression control. Nature 473 (7347), 337–342.
Serdiuk, T., Steudle, A., Mari, S.A., Manioglu, S., Kaback, H.R., Kuhn, A., Müller, D.J., 2019. Insertion and folding pathways of single membrane proteins guided by translocases and insertases. Sci. Adv. 5 (1), eaau6824.
Shafiei, G., Baillet, S., Misic, B., 2022. Human electromagnetic and haemodynamic networks systematically converge in unimodal cortex and diverge in transmodal cortex. PLoS Biol. 20 (8), e3001735.
Shafiei, G., Bazinet, V., Dadar, M., Manera, A.L., Collins, D.L., Dagher, A., Borroni, B., Sanchez-Valle, R., Moreno, F., Laforce, R., et al., 2022. Network structure and transcriptomic vulnerability shape atrophy in frontotemporal dementia. Brain.
Shafiei, G., Markello, R.D., Makowski, C., Talpalaru, A., Kirschner, M., Devenyi, G.A., Guma, E., Hagmann, P., Cashman, N.R., Lepage, M., et al., 2020. Spatial patterning of tissue volume loss in schizophrenia reflects brain network architecture. Biol. Psychiatry 87 (8), 727–735.
Sharma, K., Schmitt, S., Bergner, C.G., Tyanova, S., Kannaiyan, N., Manrique-Hoyos, N., Kongi, K., Cantuti, L., Hanisch, U.-K., Philips, M.-A., et al., 2015. Cell type–and brain region–resolved mouse brain proteome. Nat. Neurosci. 18 (12), 1819–1831.
Shine, J.M., 2019. Neuromodulatory influences on integration and segregation in the brain. Trends Cogn. Sci. (Regul. Ed.) 23 (7), 572–583.
Shine, J.M., Breakspear, M., Bell, P.T., Martens, K.A.E., Shine, R., Koyejo, O., Sporns, O., Poldrack, R.A., 2019. Human cognition involves the dynamic integration of neural activity and neuromodulatory systems. Nat. Neurosci. 22 (2), 289–296.
Smart, K., Cox, S.M., Scala, S.G., Tippler, M., Jaworska, N., Boivin, M., Séguin, J.R., Benkelfat, C., Leyton, M., 2019. Sex differences in [11 c] abp688 binding: a positron emission tomography study of mglu5 receptors. Eur. J. Nucl. Med. Mol. Imaging 46 (5), 1179–1183.
Smith, R.E., Tournier, J.-D., Calamante, F., Connelly, A., 2015. Sift2: enabling dense quantitative assessment of brain white matter connectivity using streamlines tractography. Neuroimage 119, 338–351.
Suárez, L.E., Markello, R.D., Betzel, R.F., Misic, B., 2020. Linking structure and function in macroscale brain networks. Trends Cogn. Sci..
Tournier, J.D., Calamante, F., Connelly, A., et al., 2010. Improved probabilistic streamlines tractography by 2nd order integration over fibre orientation distributions. In: Proceedings of the international society for magnetic resonance in medicine, Vol. 1670. John Wiley & Sons, Inc. New Jersey, USA.
Tournier, J.-D., Smith, R., Raffelt, D., Tabbara, R., Dhollander, T., Pietsch, M., Christiaens, D., Jeurissen, B., Yeh, C.-H., Connelly, A., 2019. Mrtrix3: a fast, flexible and open software framework for medical image processing and visualisation. Neuroimage 202, 116137.
Van Essen, D.C., Smith, S.M., Barch, D.M., Behrens, T.E., Yacoub, E., Ugurbil, K., Consortium, W.-M.H., et al., 2013. The wu-minn human connectome project: an overview. Neuroimage 80, 62–79.
Vázquez-Rodríguez, B., Suárez, L.E., Markello, R.D., Shafiei, G., Paquola, C., Hagmann, P., Van Den Heuvel, M.P., Bernhardt, B.C., Spreng, R.N., Misic, B., 2019. Gradients of structure–function tethering across neocortex. Proc. Natl. Acad. Sci. 116 (42), 21219–21227.
de Wael, R.V., Larivière, S., Caldairou, B., Hong, S.-J., Margulies, D.S., Jefferies, E., Bernasconi, A., Smallwood, J., Bernasconi, N., Bernhardt, B.C., 2018. Anatomical and microstructural determinants of hippocampal subfield functional connectome embedding. Proc. Natl. Acad. Sci. 115 (40), 10154–10159.
Wang, Z., Gerstein, M., Snyder, M., 2009. Rna-seq: a revolutionary tool for transcriptomics. Nat. Rev. Genet. 10 (1), 57–63.
Yudowski, G.A., Puthenveedu, M.A., von Zastrow, M., 2006. Distinct modes of regulated receptor insertion to the somatodendritic plasma membrane. Nat. Neurosci. 9 (5), 622–627.
Zhang, Y., Chen, K., Sloan, S.A., Bennett, M.L., Scholze, A.R., O'Keeffe, S., Phatnani, H.P., Guarnieri, P., Caneda, C., Ruderisch, N., et al., 2014. An rna-sequencing transcriptome and splicing database of glia, neurons, and vascular cells of the cerebral cortex. J. Neurosci. 34 (36), 11929–11947.
Zhou, F.C., Tao-Cheng, J.-H., Segu, L., Patel, T., Wang, Y., 1998. Serotonin transporters are located on the axons beyond the synaptic junctions: anatomical and functional evidence. Brain Res. 805 (1–2), 241–254.
Zilles, K., Palomero-Gallagher, N., 2017. Multiple transmitter receptors in regions and layers of the human cerebral cortex. Front. Neuroanat. 11, 78.
Zilles, K., Palomero-Gallagher, N., Grefkes, C., Scheperjans, F., Boy, C., Amunts, K., Schleicher, A., 2002. Architectonics of the human cerebral cortex and transmitter receptor fingerprints: reconciling functional neuroanatomy and neurochemistry. Eur. Neuropsychopharmacol. 12 (6), 587–599.
Zilles, K., Schleicher, A., Palomero-Gallagher, N., Amunts, K., 2002. Quantitative Analysis of Cyto-and Receptor Architecture of the Human Brain. In: Brain mapping: the methods. Elsevier, pp. 573–602.

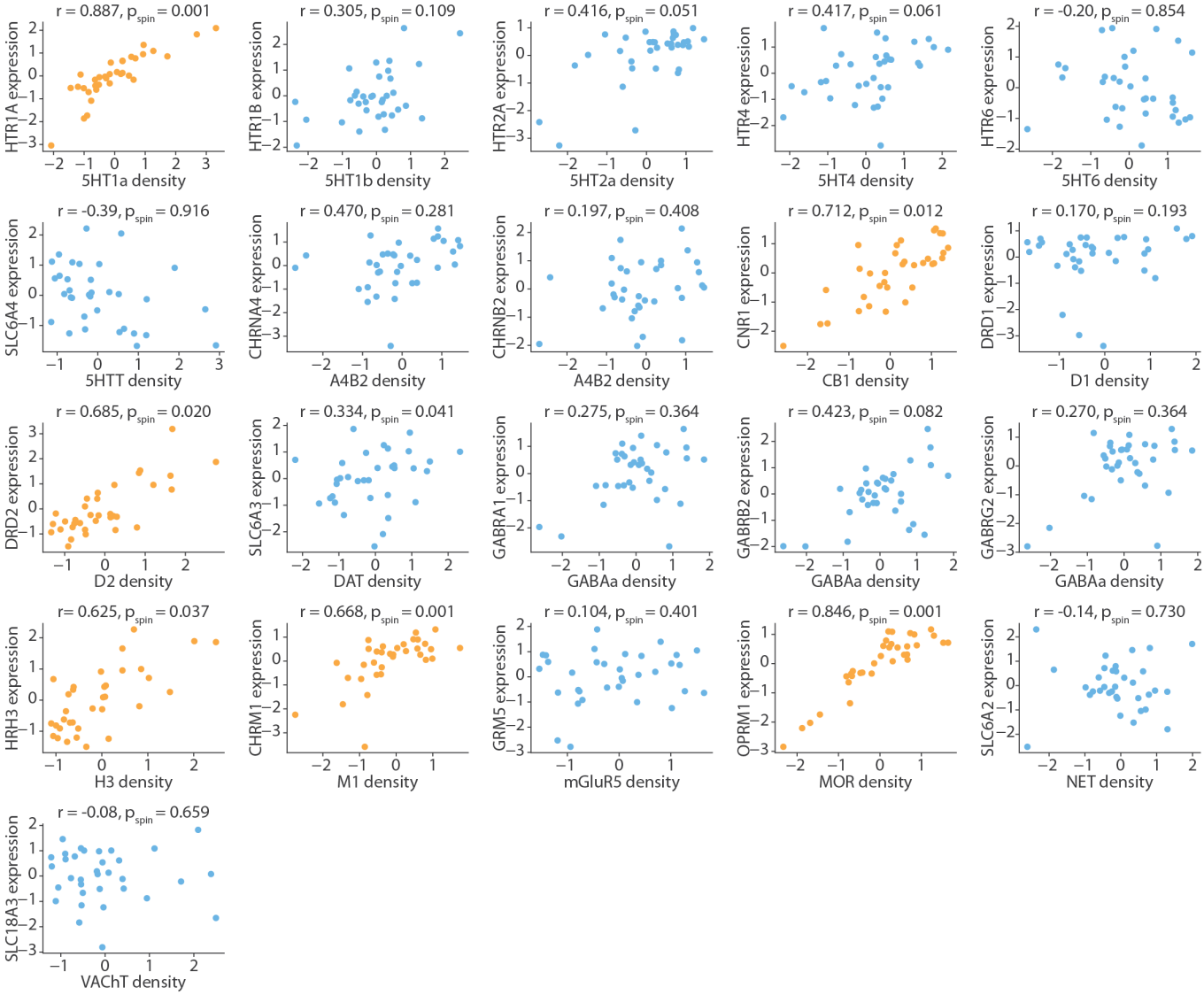

Figure S1. **PET-derived receptor densities versus RNAseq gene expression |** The analysis in Fig. 1 of the main text were repeated using RNAseq data instead of microarray gene expression [47]. Yellow scatter plots indicate significant ($p_{\text{spin}} < 0.05$) and large ($r > 0.5$) expression-density correspondence. Receptor density and gene expression is z-scored.

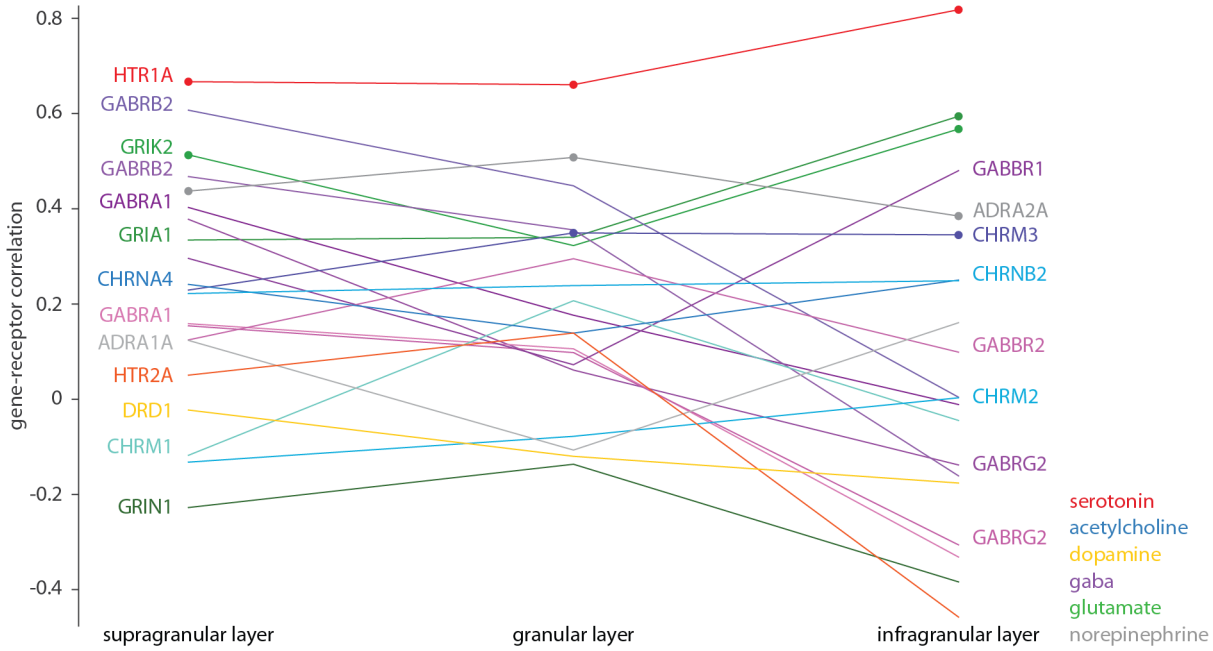

Figure S2. **Gene-receptor correlations in different laminar layers |** Gene-receptor Spearman correlation coefficients are shown in supragranular, granular, and infragranular laminar layers. Receptor density data is acquired from autoradiography [117]. Each line is associated with a gene (gene name either on the right or left of the line). Neurotransmitter systems are colour-coded according to the legend, and points refer to significant Spearman correlations ($p_{\text{spin}} < 0.05$).

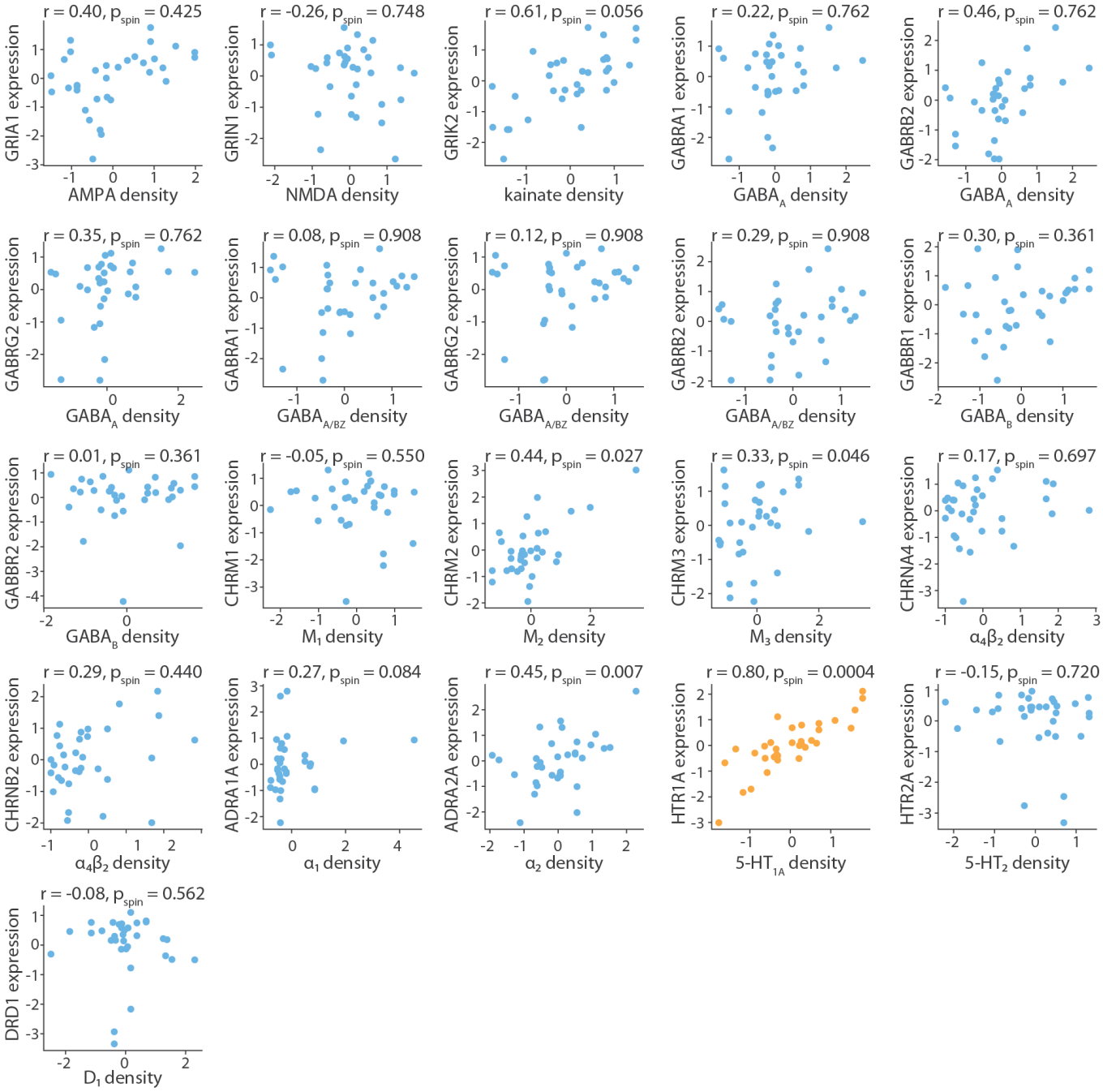

Figure S3. **Autoradiography-derived receptor densities versus RNAseq gene expression** | The analysis in Fig. 2 of the main text were repeated using RNAseq data instead of microarray gene expression [47]. Yellow scatter plots indicate significant ($p_{\text{spin}} < 0.05$) and large ($r > 0.5$) expression-density correspondence. Receptor density and gene expression is z-scored.

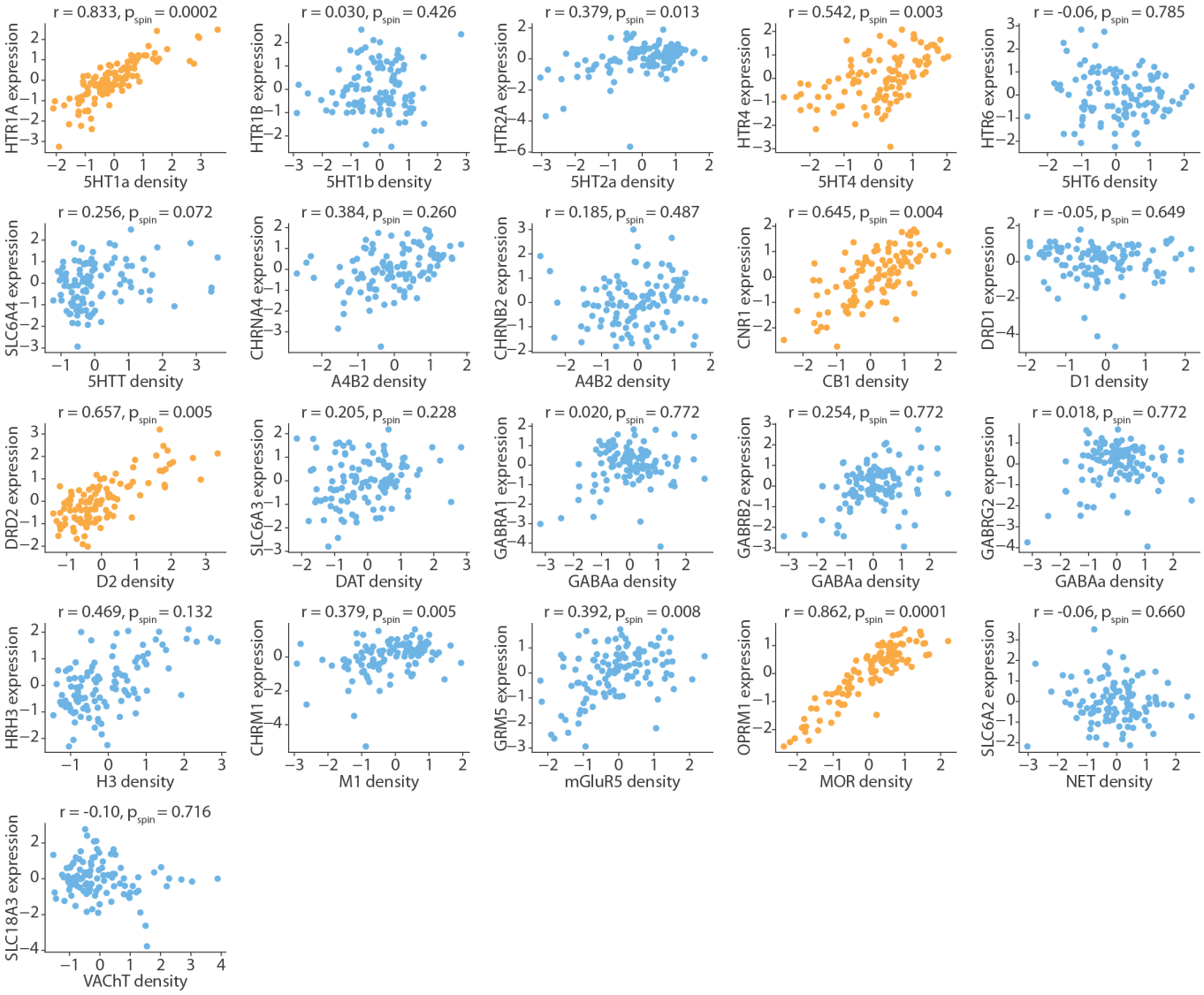

Figure S4. **Replication in a 111-node parcellation |** PET receptor/transporter densities and gene expression levels were parcellated into a 111-node cortical left hemisphere parcellation. Yellow scatter plots indicate significant ($p_{\text{spin}} < 0.05$) and large ($r > 0.5$) expression-density correspondence. Receptor density and gene expression is z-scored.

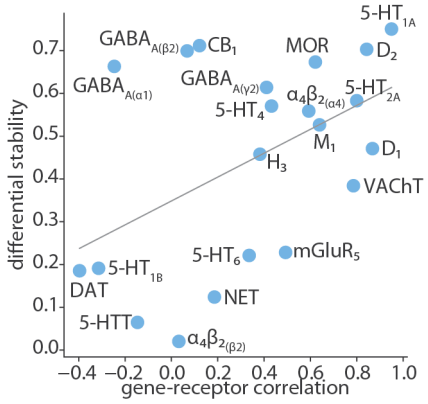

Figure S5. **Relationship between receptor expression-density correlation and differential stability in the subcortex |** We repeat Fig. 4 in the main text using the correlation between receptor gene expression and PET-derived protein density in the subcortex ($r = 0.46$, $p = 0.038$). Notably, expression-density relationships for some receptors (e.g. VAChT, D_1, and 5-HT_6) considerably improve in the subcortex despite low differential stability. This may be due to a smaller distance between mRNA transcripts and protein expression on the cell surface, or differences in PET radioligand binding in subcortex versus cortex (as is the case for D_1 which shows improved binding specificity in the subcortex [34]).

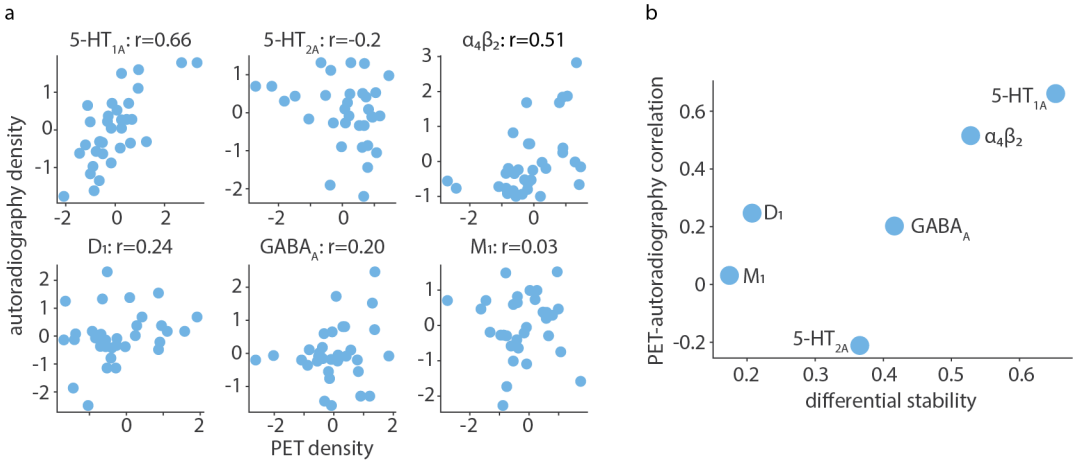

Figure S6. **Correspondence between PET- and autoradiography-derived receptor density |** (a) Spearman correlation between PET- and autoradiography-derived receptor density for the six receptors with both measurements. (b) The relationship between genetic differential stability and the PET-autoradiography correspondence for the same six receptors.

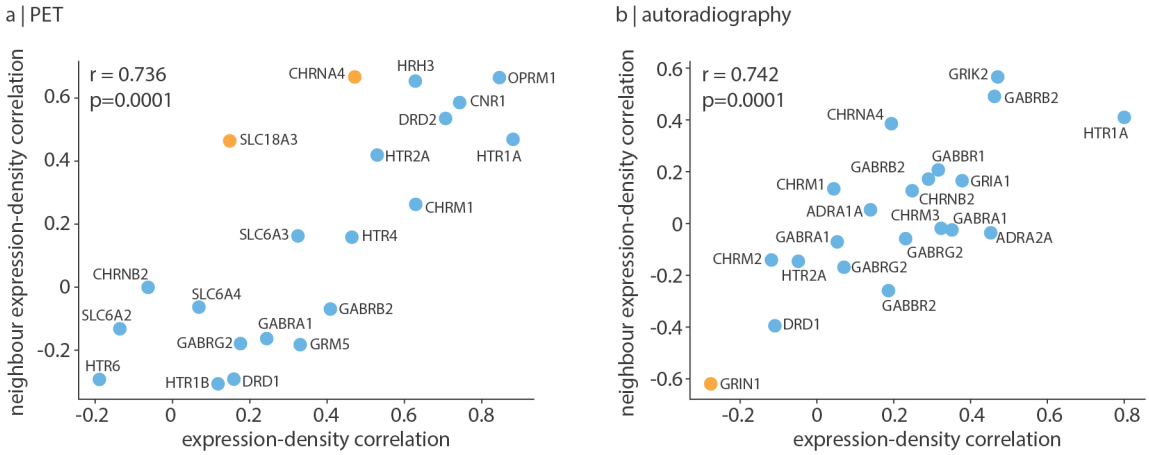

Figure S7. **Correspondence between regional receptor density and neighbouring gene expression |** For each gene-receptor pair, we correlate regional receptor density with the mean gene expression of structurally-connected neighbours, weighted by the structural connection (x-axis). Yellow points indicate significant (two-tailed $p_{\text{spin}} < 0.05$) correlations between regional receptor density and neighbouring gene expression. Next, we plot the region-neighbour correlation against the original correlation between gene expression and receptor density. This analysis was conducted using (a) PET-derived receptor density and (b) autoradiography-derived receptor density.

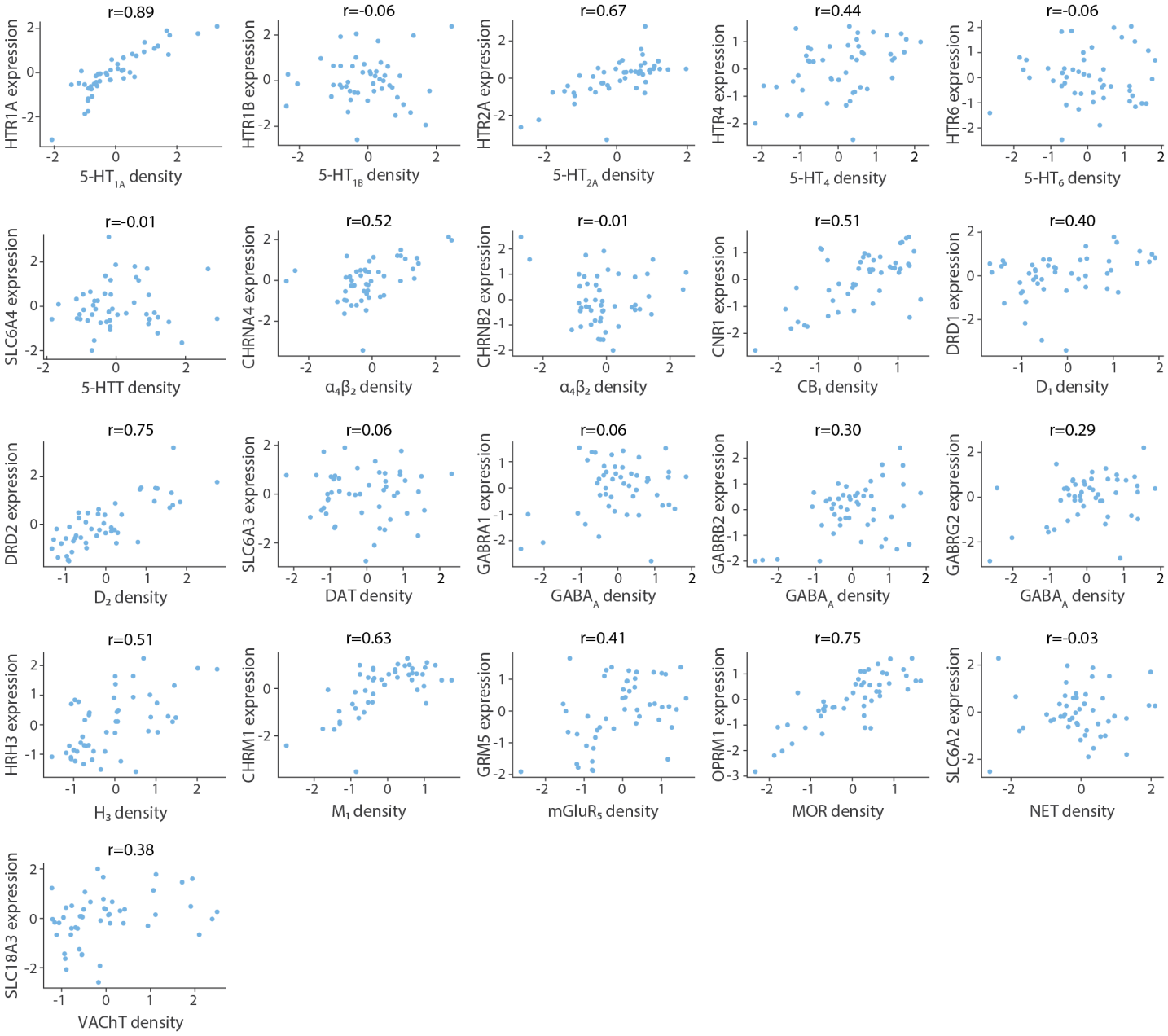

Figure S8. **PET-derived whole-brain expression-density correspondence |** For each gene-receptor pair, we separately z-score cortical and subcortical gene expression and receptor density. Then, we combine all regions into a single analysis and compare whole-brain gene expression to receptor density.

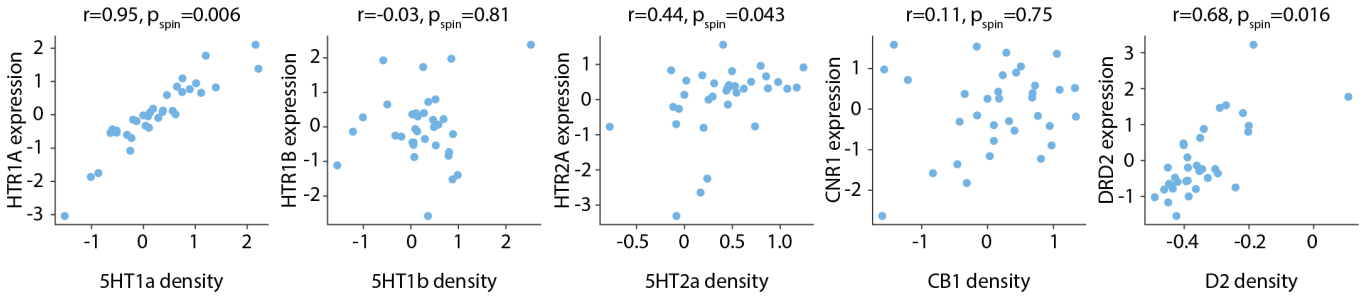

Figure S9. **Alternative PET tracer choices |** For completeness, we repeat the analysis using alternative PET tracers, which is available for five receptors: 5-HT_{1A} ([^{11}C]CUMI-101 [11]), 5-HT_{1B} ([^{11}C]AZ10419369 [11]), 5-HT_{2A} ([^{18}F]altanserin [94]), CB_1 ([^{18}F]FMPEP-D2 [59]), and D_2 ([^{18}F]fallypride [51]).

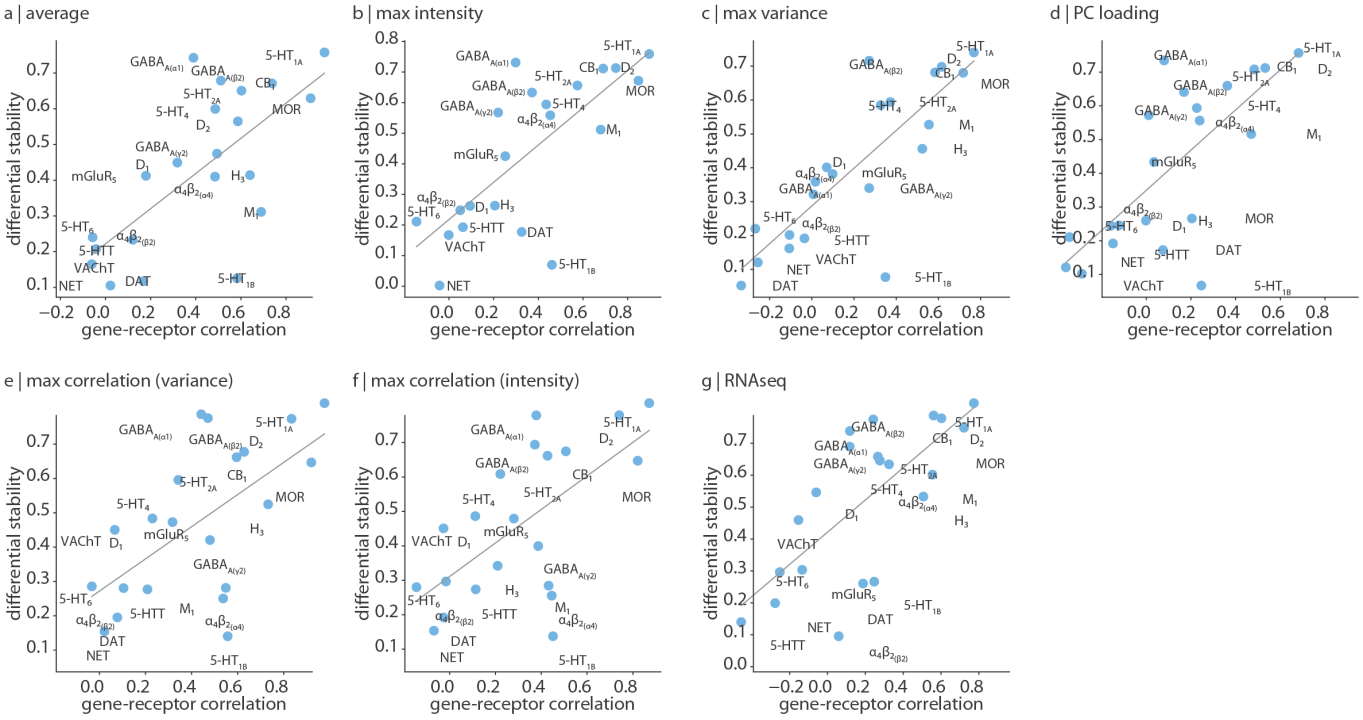

Figure S10. **Comparing probe-selection method |** The relationship between receptor expression-density correspondence and differential stability is conserved when (a) all microarray probes indexing the same gene are averaged together (Spearman $r = 0.55$, $p = 0.009$), (b) the selected probe has maximum average expression (Spearman $r = 0.68$, $p = 0.0007$), (c) the selected probe has maximum variance in expression (Spearman $r = 0.74$, $p = 0.0001$), (d) the selected probe has maximum loading on the first principal component of gene expression (Spearman $r = 0.66$, $p = 0.001$), (e) the selected probe is maximally correlated to other probes from the same gene (if only one probe exists, the maximum variance as in (c) is selected instead; Spearman $r = 0.49$, $p = 0.024$), (f) the selected probe is maximally correlated to other probes from the same gene (if only one probe exists, the maximum intensity as in (b) is selected instead; Spearman $r = 0.55$, $p = 0.010$), and (g) the selected probe has the most consistent pattern of regional variation to RNAseq data (Spearman $r = 0.71$, $p = 0.0003$) [62].

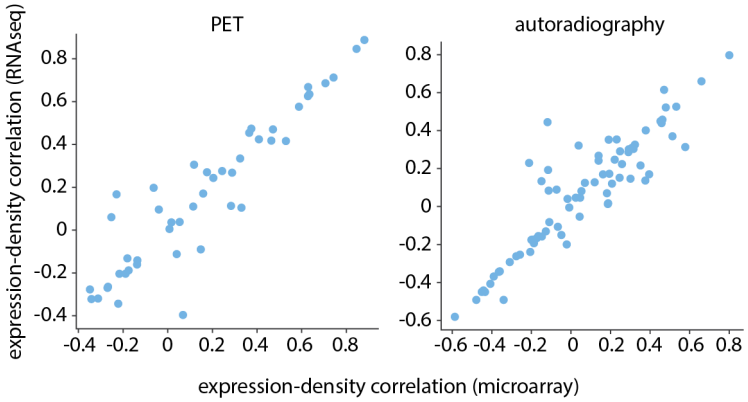

Figure S11. **Microarray versus RNAseq AHBA gene expression |** We plot that expression-density correlation computed for all gene-receptor pairs when calculated using microarray versus RNAseq AHBA gene expression. Each point represents a gene-receptor pair.

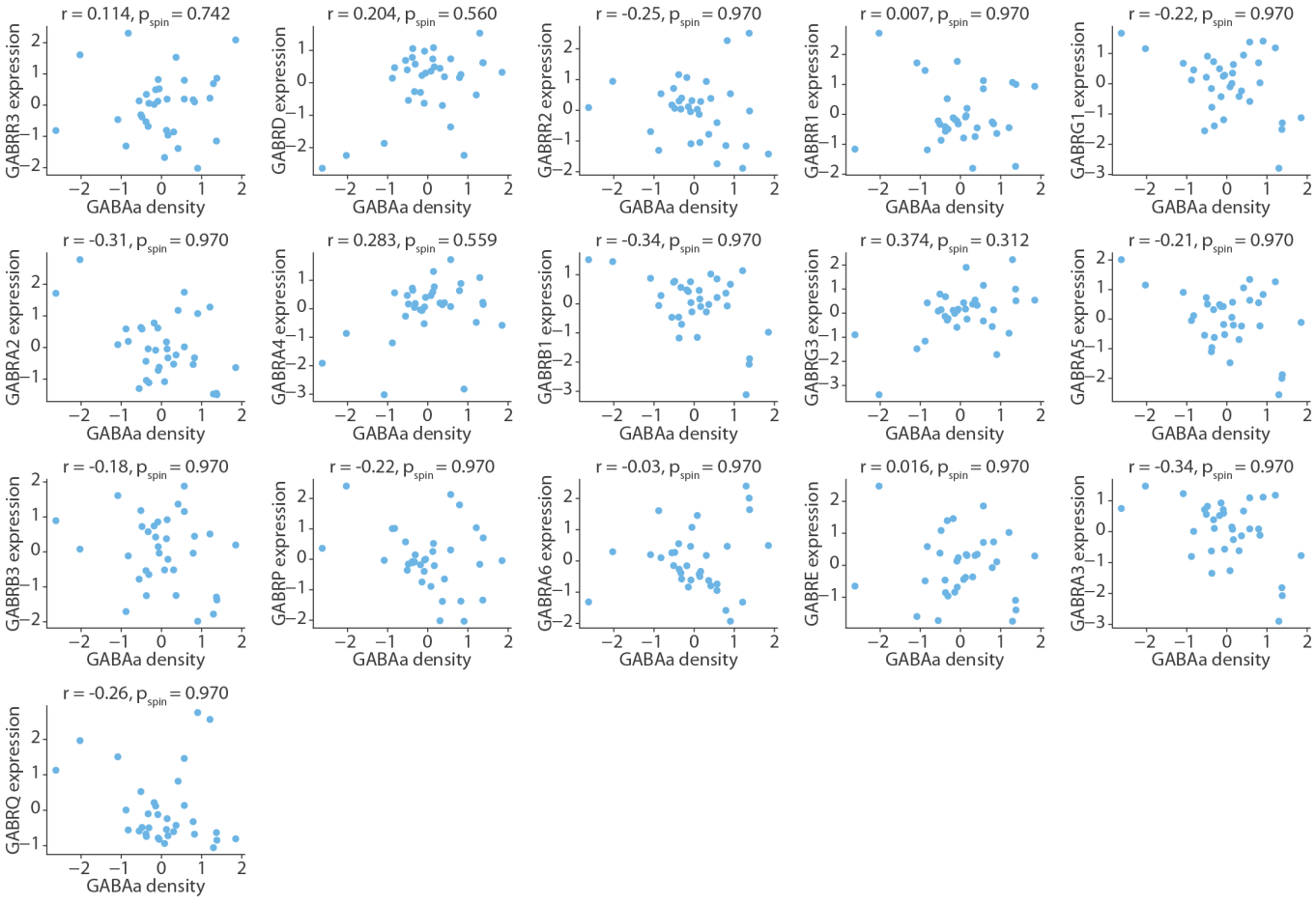

Figure S12. **Expression-density association for the remaining sixteen GABAa subunits |** Expression-density association for the remaining sixteen GABAa subunits that do not comprise the main channel (α_1, β_2, γ_2), after correcting for multiple comparisions (FDR). Receptor density and gene expression is z-scored.

Receptor/ transporter	Neurotransmitter	Tracer	Measure	N	Age	References
D_1	dopamine	[^{11}C]SCH23390	BP_{ND}	13	33 ± 13	Kaller et al., 2017 [54]
D_2	dopamine	[^{11}C]FLB-457	BP_{ND}	37	48.4 ± 16.9	Smith et al., 2019 [91, 105]
D_2	dopamine	[^{11}C]FLB-457	BP_{ND}	55	32.5 ± 9.7	Sandiego et al., 2015 [91, 92, 103, 105, 114]
D_2	dopamine	[^{11}C]raclopride	BP_{ND}	7	24 ± 2	Alakurtti et al., 2015 [2]
DAT*	dopamine	[^{123}I]-FP-CIT	SUVR	174	61 ± 11	Dukart et al., 2018 [31]
NET*	norepinephrine	[^{11}C]MRB	BP_{ND}	77	33.4 ± 9.2	Ding et al., 2010 [10, 21, 29, 90]
5-HT_{1A}	serotonin	[^{11}C]WAY-100635	BP_{ND}	36	26.3 ± 5.2	Savli et al., 2012 [94]
5-HT_{1B}	serotonin	[^{11}C]P943	BP_{ND}	65	33.7 ± 9.7	Gallezot et al., 2010 [6, 39, 66, 71, 72, 82, 93]
5-HT_{1B}	serotonin	[^{11}C]P943	BP_{ND}	23	28.7 ± 7.0	Savli et al., 2012 [94]
5-HT_{2A}	serotonin	[^{11}C]Cimbi-36	B_{max}	29	22.6 ± 2.7	Beliveau et al., 2017 [11]
5-HT_4	serotonin	[^{11}C]SB207145	B_{max}	59	25.9 ± 5.3	Beliveau et al., 2017 [11]
5-HT_6	serotonin	[^{11}C]GSK215083	BP_{ND}	30	36.6 ± 9.0	Radhakrishnan et al., 2018 [85, 86]
5-HTT*	serotonin	[^{11}C]DASB	B_{max}	100	25.1 ± 5.8	Beliveau et al., 2017 [11]
$\alpha_4\beta_2$	acetylcholine	[^{18}F]flubatine	V_T	30	33.5 ± 10.7	Hillmer et al., 2016 [5, 48]
M_1	acetylcholine	[^{11}C]LSN3172176	BP_{ND}	24	40.5 ± 11.7	Naganawa et al., 2021 [73]
VAChT*	acetylcholine	[^{18}F]FEOBV	SUVR	4	37 ± 10.2	PI: Lauri Tuominen & Synthia Guimond [44]
VAChT*	acetylcholine	[^{18}F]FEOBV	SUVR	18	66.8 ± 6.8	Aghourian et al., 2017 [1]
VAChT*	acetylcholine	[^{18}F]FEOBV	SUVR	5	68.3 ± 3.1	Bedard et al., 2019 [9]
VAChT*	acetylcholine	[^{18}F]FEOBV	SUVR	3	66.6 ± 0.94	PI: Taylor W. Schmitz & R. Nathan Spreng [44]
$mGluR_5$	glutamate	[^{11}C]ABP688	BP_{ND}	73	19.9 ± 3.04	Smart et al., 2019 [104]
$mGluR_5$	glutamate	[^{11}C]ABP688	BP_{ND}	22	67.9 ± 9.6	PI: Pedro Rosa-Neto [44]
$mGluR_5$	glutamate	[^{11}C]ABP688	BP_{ND}	28	33.1 ± 11.2	DuBois et al., 2016 [30]
$GABA_{A/BZ}$	GABA	[^{11}C]flumazenil	B_{max}	16	26.6 ± 8	Nørgaard et al., 2021 [75]
H_3	histamine	[^{11}C]GSK189254	V_T	8	31.7 ± 9.0	Gallezot et al., 2017 [40]
CB_1	cannabinoid	[^{11}C]OMAR	V_T	77	30.0 ± 8.9	Normandin et al., 2015 [33, 74, 77, 87]
MOR	opioid	[^{11}C]carfentanil	BP_{ND}	204	32.3 ± 10.8	Kantonen et al., 2020 [55]

TABLE S1. **Neurotransmitter receptors and transporters included in analyses |** BP_{ND} = non-displaceable binding potential; V_T = tracer distribution volume; B_{max} = density (pmol/ml) converted from binding potential (5-HT) or distributional volume (GABA) using autoradiography-derived densities; SUVR = standard uptake value ratio. Refer to [44] for more details. Note that [^{11}C]raclopride is used to map subcortical D_2 density while [^{11}C]FLB-457 is used to map cortical D_2 density. Asterisks indicate transporters.

Receptor	Neurotransmitter	Excitatory/Inhibitory	Ionotropic/Metabotropic
AMPA	glutamate	excitatory	ionotropic
NMDA	glutamate	excitatory	ionotropic
Kainate	glutamate	excitatory	ionotropic
$GABA_A$	GABA	inhibitory	ionotropic
$GABA_{A/BZ}$	GABA	inhibitory	ionotropic
$GABA_B$	GABA	inhibitory	metabotropic
M_1	acetylcholine	excitatory	metabotropic
M_2	acetylcholine	inhibitory	metabotropic
M_3	acetylcholine	excitatory	metabotropic
$\alpha_4\beta_2$	acetylcholine	excitatory	ionotropic
α_1	norepinephrine	excitatory	metabotropic
α_2	norepinephrine	inhibitory	metabotropic
5-HT_{1A}	serotonin	inhibitory	metabotropic
5-HT_2	serotonin	excitatory	metabotropic
D_1	dopamine	excitatory	metabotropic

TABLE S2. **Neurotransmitter receptors included in the autoradiography dataset**

gene	receptor	Spearman r	p_{spin}	gene	receptor	Spearman r	p_{spin}
HTR1A	5HT1a	0.795875	0.009299	GABRG2	GABAa	0.155691	0.805419
HTR1B	5HT1b	0.153247	0.425057	GABRR3	GABAa	0.089381	0.805419
HTR2A	5HT2a	0.166692	0.489651	GABRD	GABAa	0.241864	0.797034
HTR4	5HT4	0.445684	0.099290	GABRR2	GABAa	-0.067991	0.802279
HTR6	5HT6	-0.188999	0.330967	GABRR1	GABAa	-0.101910	0.797034
SLC6A4	5HTT	0.061574	0.722628	GABRG1	GABAa	-0.539190	0.381319
CHRNA2	A4B2	0.053323	0.802520	GABRA2	GABAa	-0.557830	0.381319
CHRNA3	A4B2	-0.267532	0.778172	GABRA4	GABAa	0.131551	0.802279
CHRNA4	A4B2	0.471352	0.558194	GABRB1	GABAa	-0.528801	0.381319
CHRNA5	A4B2	0.365011	0.347565	GABRG3	GABAa	0.423682	0.381319
CHRNA6	A4B2	0.587777	0.152335	GABRA5	GABAa	-0.521772	0.381319
CHRNA7	A4B2	0.288312	0.761564	GABRB3	GABAa	-0.369595	0.414729
CHRNA9	A4B2	-0.175248	0.788621	GABRP	GABAa	-0.460963	0.381319
CHRNA10	A4B2	-0.137357	0.802520	GABRA6	GABAa	0.246448	0.797034
CHRNB2	A4B2	-0.063102	0.802520	GABRE	GABAa	-0.274255	0.778749
CHRNB3	A4B2	0.634530	0.096790	GABRA3	GABAa	-0.416043	0.394738
CHRNB4	A4B2	0.040183	0.802520	GABRQ	GABAa	-0.464629	0.394738
CNR1	CB1	0.742704	0.051995	HRH3	H3	0.628113	0.133387
DRD1	D1	0.138273	0.496950	CHRM1	M1	0.629030	0.001700
DRD2	D2	0.699007	0.038696	GRM5	mGluR5	0.343621	0.118588
SLC6A3	DAT	0.280672	0.185981	OPRM1	MOR	0.802903	0.001800
GABRA1	GABAa	0.245531	0.797034	SLC6A2	NET	-0.136134	0.523948
GABRB2	GABAa	0.525439	0.381319	SLC18A3	VAChT	0.129412	0.473253

TABLE S3. Spearman correlations between microarray gene expression and PET-derived receptor density in the cortex. Significance was assessed against a spatial autocorrelation preserving null model (p_{spin}) and in cases where receptors are repeated, corrected for multiple comparisons [12].

gene	receptor	Spearman r	p	gene	receptor	Spearman r	p
HTR1A	5HT1a	0.950000	3.043129×10^{-08}	GABRG2	GABAa	0.410714	6.416432×10^{-02}
HTR1B	5HT1b	-0.314286	8.730300×10^{-01}	GABRR3	GABAa	-0.253571	8.190919×10^{-01}
HTR2A	5HT2a	0.800000	1.711349×10^{-04}	GABRD	GABAa	0.182143	2.579408×10^{-01}
HTR4	5HT4	0.432143	5.384652×10^{-02}	GABRR2	GABAa	-0.060714	5.850940×10^{-01}
HTR6	5HT6	0.335714	1.106058×10^{-01}	GABRR1	GABAa	-0.564286	9.857837×10^{-01}
SLC6A4	5HTT	-0.146429	6.987250×10^{-01}	GABRG1	GABAa	0.360714	9.327719×10^{-02}
CHRNA2	A4B2	0.639286	5.144223×10^{-03}	GABRA2	GABAa	0.507143	2.683183×10^{-02}
CHRNA3	A4B2	0.425000	5.714774×10^{-02}	GABRA4	GABAa	0.467857	3.931512×10^{-02}
CHRNA4	A4B2	0.592857	9.923211×10^{-03}	GABRB1	GABAa	0.735714	8.849343×10^{-04}
CHRNA5	A4B2	0.342857	1.054619×10^{-01}	GABRG3	GABAa	0.567857	1.361418×10^{-02}
CHRNA6	A4B2	0.350000	1.004727×10^{-01}	GABRA5	GABAa	0.610714	7.796416×10^{-03}
CHRNA7	A4B2	-0.157143	7.120237×10^{-01}	GABRB3	GABAa	0.532143	2.057929×10^{-02}
CHRNA9	A4B2	-0.278571	8.426453×10^{-01}	GABRP	GABAa	-0.150000	7.031849×10^{-01}
CHRNA10	A4B2	-0.575000	9.875319×10^{-01}	GABRA6	GABAa	0.335714	1.106058×10^{-01}
CHRNB2	A4B2	0.032143	4.547311×10^{-01}	GABRE	GABAa	0.200000	2.374070×10^{-01}
CHRNB3	A4B2	-0.075000	6.047446×10^{-01}	GABRA3	GABAa	0.328571	1.159048×10^{-01}
CHRNB4	A4B2	-0.375000	9.157836×10^{-01}	GABRQ	GABAa	0.439286	5.068029×10^{-02}
CNR1	CB1	0.121429	3.332006×10^{-01}	HRH3	H3	0.382143	7.991181×10^{-02}
DRD1	D1	0.867857	1.375903×10^{-05}	CHRM1	M1	0.639286	5.144223×10^{-03}
DRD2	D2	0.842857	3.983598×10^{-05}	GRM5	mGluR5	0.492857	3.097550×10^{-02}
SLC6A3	DAT	-0.396429	9.282527×10^{-01}	OPRM1	MOR	0.621429	6.701003×10^{-03}
GABRA1	GABAa	-0.246429	8.120247×10^{-01}	SLC6A2	NET	0.185714	2.537705×10^{-01}
GABRB2	GABAa	0.067857	4.050544×10^{-01}	SLC18A3	VAChT	0.785714	2.582274×10^{-04}

TABLE S4. Spearman correlations between microarray gene expression and PET-derived receptor density in the subcortex. In cases where receptors are repeated, parametric p-values were corrected for multiple comparisons [12].

gene	receptor	Spearman r	p_{spin}	gene	receptor	Spearman r	p_{spin}
GRIA1	AMPA	0.378166	0.637403	GABRR3	GABAa/BZ	-0.126891	0.865499
GRIA2	AMPA	0.207473	0.637403	GABRD	GABAa/BZ	0.162000	0.943870
GRIA3	AMPA	-0.017220	0.830617	GABRR2	GABAa/BZ	0.190922	0.865499
GRIA4	AMPA	0.300928	0.637403	GABRR1	GABAa/BZ	-0.164674	0.865499
GRIN1	NMDA	-0.276352	0.774923	GABRG1	GABAa/BZ	-0.196272	0.933163
GRIN2A	NMDA	-0.148792	0.774923	GABRA2	GABAa/BZ	-0.309120	0.865499
GRIN2B	NMDA	0.257962	0.774923	GABRA4	GABAa/BZ	0.245925	0.865499
GRIN2C	NMDA	0.139597	0.774923	GABRB1	GABAa/BZ	-0.359609	0.865499
GRIN2D	NMDA	-0.112681	0.774923	GABRG3	GABAa/BZ	0.181894	0.865499
GRIN3A	NMDA	-0.188581	0.774923	GABRA5	GABAa/BZ	-0.478308	0.865499
GRIN3B	NMDA	0.292234	0.774923	GABRB3	GABAa/BZ	-0.364290	0.865499
GRIK1	kainate	0.479478	0.325634	GABRP	GABAa/BZ	-0.211485	0.865499
GRIK2	kainate	0.470785	0.325634	GABRA6	GABAa/BZ	0.395386	0.865499
GRIK3	kainate	0.458246	0.325634	GABRE	GABAa/BZ	-0.146953	0.933163
GRIK4	kainate	0.188080	0.725027	GABRA3	GABAa/BZ	-0.450556	0.865499
GRIK5	kainate	0.309120	0.445080	GABRQ	GABAa/BZ	-0.407256	0.865499
GABRA1	GABAa	0.351584	0.866313	GABBR1	GABAb	0.316141	0.361764
GABRB2	GABAa	0.462259	0.866313	GABBR2	GABAb	0.186408	0.361764
GABRG2	GABAa	0.231046	0.884150	CHRM1	m1	0.043969	0.842216
GABRR3	GABAa	0.119870	0.884150	CHRM2	m2	-0.118365	0.678632
GABRD	GABAa	0.221182	0.884150	CHRM3	m3	0.323497	0.097890
GABRR2	GABAa	0.038786	0.970003	CHRNA2	a4b2	-0.008526	0.999400
GABRR1	GABAa	-0.173034	0.866313	CHRNA3	a4b2	0.046477	0.999400
GABRG1	GABAa	-0.205634	0.884150	CHRNA4	a4b2	0.193931	0.999400
GABRA2	GABAa	-0.340216	0.884150	CHRNA5	a4b2	-0.072557	0.999400
GABRA4	GABAa	0.375993	0.866313	CHRNA6	a4b2	0.532308	0.654985
GABRB1	GABAa	-0.390036	0.884150	CHRNA7	a4b2	-0.066204	0.999400
GABRG3	GABAa	0.577782	0.714329	CHRNA9	a4b2	-0.257628	0.999400
GABRA5	GABAa	-0.434172	0.866313	CHRNA10	a4b2	-0.187077	0.999400
GABRB3	GABAa	-0.199783	0.884150	CHRNB2	a4b2	0.248098	0.999400
GABRP	GABAa	-0.115523	0.884150	CHRNB3	a4b2	0.659701	0.252975
GABRA6	GABAa	0.513082	0.866313	CHRNB4	a4b2	-0.021232	0.999400
GABRE	GABAa	0.024241	0.884150	ADRA1A	a1	0.139597	0.571443
GABRA3	GABAa	-0.586642	0.714329	ADRA2A	a2	0.452562	0.027897
GABRQ	GABAa	-0.442030	0.866313	HTR1A	5-HT1a	0.800301	0.001700
GABRA1	GABAa/BZ	0.052997	0.984302	HTR2A	5-HT2	-0.048316	0.824618
GABRB2	GABAa/BZ	0.290395	0.865499	DRD1	D1	-0.109337	0.801820
GABRG2	GABAa/BZ	0.070551	0.984302				

TABLE S5. Spearman correlations between microarray gene expression and autoradiography-derived receptor density. Significance was assessed against a spatial autocorrelation preserving null model (p_{spin}) and in cases where receptors are repeated, corrected for multiple comparisons [12].

receptor	# AHBA genes	# significant	gene names	# r>0.5
$5HT_{1A}$	18.0	2.0	*HTR2C*, *HTR1A*	3
$5HT_{1B}$	18.0	0.0		0
$5HT_{2A}$	18.0	0.0		3
$5HT_4$	18.0	3.0	*HTR2C*, *HTR3B*, *HTR1A*	4
$5HT_6$	18.0	0.0		0
5HTT	18.0	0.0		0
$\alpha_4\beta_2$	181.0	0.0		18
M_1	181.0	0.0		4
VAChT	181.0	0.0		1
CB_1	26.0	7.0	*GNB2*, *GNB4*, *CNR1*, *CNRIP1*, *GRM1*, *GNG4*, *PLCB2*	10
D_1	71.0	0.0		3
D_2	71.0	0.0		11
DAT	71.0	0.0		2
$GABA_A$	70.0	0.0		2
H_3	62.0	0.0		4
$mGluR_5$	171.0	0.0		0
MOR	47.0	4.0	*ADCY2*, *GNB2*, *GNB4*, *OPRM1*	18
NET	29.0	0.0		2

TABLE S6. **Panther ontology pathways |** For each neurotransmitter receptor, we used the Panther classification system to construct a list of genes related to proteins within the neurotransmitter's protein pathway (using the neurotransmitter's name as a search term, e.g. "dopamine"). Here we show the number of genes in each list, the number and names of genes that are significantly correlated with PET-derived protein density (FDR-correct $p_{\text{spin}} < 0.05$), and then number of genes that show large correlation ($r > 0.5$) with PET-derived protein density, irregardless of statistical significance.